Estimation of solar irradiance at the North Sea using machine learning

University of Utrecht

Energy Science, Copernicus Institute

MSc Thesis

Stef Knibbeler

6203485

Supervisors   Tarek Alskaif & Lennard Visser

Co-accessor   Vinzenz de Koning

Date of submission: 22 April 2019

1 Abstract

Further integration of renewable energy will result in higher pressure on land availability especially in densely populated areas. Therefore, several companies are exploring the possibility of offshore PV systems. To estimate the potential of offshore PV in the North Sea, this research provides an offshore irradiance estimation. This estimation is conducted comparing the Machine Learning Methods (MLMs), Random forest (RF), Extreme Gradient Boosting (XGB) and the Artificial Neural Network (ANN). The estimation is performed using onshore training data provided by the Royal Dutch Meteorological Institute (KNMI) containing 15 different climate variables as input for the MLMs. This research presents a new approach in the solar resource estimation field by evaluating the role of external factors that influence the performance of the selected MLMs. An onshore case study is conducted to identify how the distance, cardinal direction and temporal differences between training and validation data affect the performance of the selected MLMs. This onshore case study is performed using data of 15 selected stations in the Netherlands. The ANN produced the overall best performance with an average MAE of 21.5 J/cm^2 and a relative error of 1.10. XGB (22.63 J/cm^2, 1.092) and RF (22.67, 1.149) produced slightly higher errors. Based on the onshore case study it is concluded that the external factors distance and cardinal direction strongly affect the performance of MLMs. Larger distances between training and validation stations resulted in considerable higher relative errors and models validated west of the training station showed above average relative errors for all MLMs. Temporal differences between training and validation data moderately affected the performance of the MLMs. The results of the offshore estimation produced average irradiance levels of 73.1 J/cm^2 which is slightly lower compared to onshore levels of 75.6 J/cm^2. These results are conflicting as a satellite based study by the KNMI concluded offshore irradiance levels are 4-8% higher compared to onshore levels. Since most offshore stations are located north-west of onshore training stations and distances are relatively large, the result of this estimation should be interpreted with caution. Considerable improvements on the offshore estimation can possibly be made by combining ground measurements with satellite data. Nevertheless, this research provides valuable conclusions on the performance of MLMs to estimate offshore irradiance.

2 Acknowledgements

I would like to thank my supervisors for their pleasant cooperation over the last months. I thank Tarek Alskaif and Lennard Visser for their thorough and constructive feedback during the process. Also, I want to thank Vinzenz Koning for his feedback on my research proposal. Furthermore, I want to thank the KNMI for their open sourced database I used to perform this research.

Contents

List of Figures

3 Introduction

Renewables are becoming competitive with fossil fuels which has induced a large scale deployment of these technologies worldwide. The total Total Primary Energy Supply (TPES) of renewables (excluding biofuels and nuclear energy) increased from around 11.9 EJ in 2000 to 24.1 EJ in 2016 (IEA, 2018). This development caused a higher pressure on land availability. As can be seen in figure 1, renewables have significantly lower power densities (W/m^2) compared to conventional energy resources. Therefore, further integration of renewables will result in higher pressure on land availability. Johansson (2013) identifies land-use as one of the key challenges of the energy transition. Especially in densely populated areas this creates new challenges for urban development.
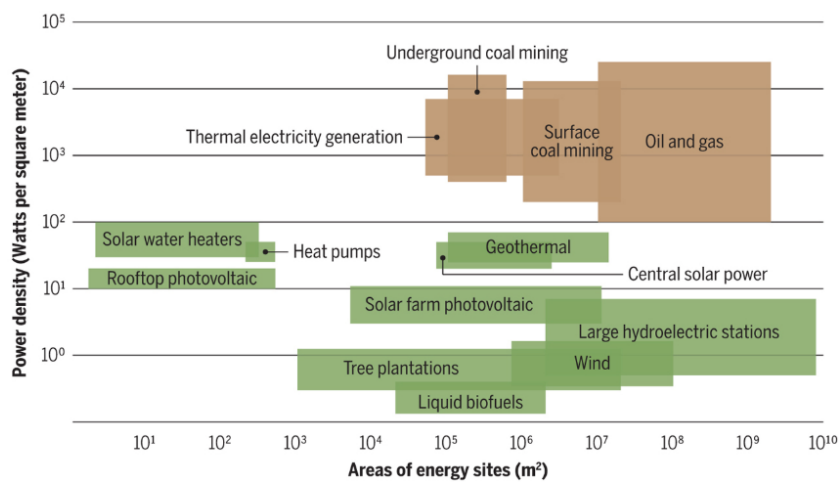
Figure 1: Power density of different energy resources. Source:(Voosen, 2018).

Nowadays around 40 % of the world's population lives within an approximate 100 km of the coast (UN, 2017). Therefore, the sea offers great potential solving land scarcity for further renewable energy integration. Offshore wind has already started to spread widely in north western Europe and became competitive to fossil fuels. In 2018, the Dutch government announced to build the first offshore wind farm without public subsidy (Wind Europe, 2018). In contrast to wind farms, solar parks parks have been only constructed on land and lakes. This has resulted in a significant increase in public resistance towards onshore solar parks in the Netherlands. According to a recent study carried out by the Wageningen University (2019), 46 percent of 45,000 people believed that agricultural land should not be used for new solar parks. Therefore, several companies are exploring the possibility to harvest the suns energy at the sea: The Norwegian company Ocean Sun has tested prototypes in Singapore and Norway with satisfactory results (PV-tech, 2018). The Dutch company, Oceans of Energy is planning to build an offshore floating PV pilot in 2019 (Oceans of Energy, 2018) and Singapore's Sunseap group announced to build a 5 MW offshore floating PV

pilot in early 2019 (Bhambhani, 2018). Offshore PV offers potential energy efficiency improvements compared to its onshore counterpart due to the cooling effect of the seawater. According to Wilfried van Sark this cooling effect could potentially increase the yield by 15 % (Utrecht University, 2018). One of the potential niches for offshore PV is the placement between existing wind farms in the North Sea because it offers several advantages:

- First of all, placement between existing wind farms could be beneficial since transmission infrastructure is already present.

- Secondly, in contrast to onshore land availability, there is an abundance of unused space between the offshore wind turbines that can be used for offshore PV.

- Thirdly, combining solar and wind could reduce the volatility in power production. Operators of offshore wind farms often observe abrupt changes in power production related to the turbulent nature of the wind (Pinson, 2008). According to Miglietta et al. (2017) wind and solar are complementary resources and therefore placing PV between existing wind farms could potentially reduce these abrupt changes in power production.

To estimate the potential of offshore PV in the North Sea, accurate data on solar irradiance is desired. Specifically for large-scale integration accurate data on irradiance is crucial (Lauret, 2015). The Royal Netherlands Meteorological Institute (KNMI) monitors onshore and offshore climate variables on a hourly resolution. A comparison of onshore and offshore irradiance data would provide new insights on the potential of offshore PV. However, the KNMI only measures solar irradiance at onshore stations. Due to the fact that hourly irradiance data is not available in the North Sea, one method is to use onshore data to determine offshore irradiance using supervised learning. In supervised learning a model is provided with a pair of input variables and the desired output (irradiance). The model produces a function that calculates the desired output based on the input variables (Voyant et al. 2017). Mellit & Pavan (2010) classified this type of learning in three categories: The first category estimates solar irradiance based on other climate variables. A second approach allows predicting the future solar irradiance based on the past observed irradiance data, and the third approach combines both to forecast solar irradiance. Since hourly irradiance data is not available in the North Sea, other climate variables are used as input to estimate solar irradiance. Consequently, Mellit and Pavan's first approach is used to estimate solar irradiance in this research.

Many studies have performed similar solar resource estimation assessments. Reddy & Ranjan (2003) concluded that Artificial Neural Networks (ANN) show promise for estimation of solar

irradiance in India where monitoring stations for irradiance are not always established. Sözen et al. (2004) concluded that ANN models could enable scientist to locate and design solar energy systems in Turkey. Gala et al. (2017) showed that Extreme Gradient Boosting (XGB) and Random Forest (RF) are quite effective and, hence, relevant for solar irradiance estimations. However, the main difference between these studies and this study is that none of the previous studies considered geographical and temporal differences that could influence the performance of the Machine Learning Methods (MLM). When onshore trained algorithms are used to estimate irradiance at offshore locations, external factors such as distance, cardinal direction and temporal differences should be taken into account.

For example, in the research of Reddy and Ranjan out of 13 stations, 11 stations were randomly selected for training purposes and the remaining two for validation. In the research of Sozen et al. out of 17 stations, 11 were used for training and 6 for validation. The results of these studies were therefore based on the accuracy's of the validation stations. The question arises if the results of these studies would have been significantly different if other stations were selected for training and validation and if the performance of the MLMs was affected by geographical and temporal differences between training and validation data. When onshore trained algorithms are used to estimate offshore irradiance these factors can potentially play an important role. Therefore, this research provides an evaluation on the performance of the MLMs RF, XGB and ANN to estimate offshore irradiance using onshore training data. In addition to similar solar resource estimations studies, in this study the legitimacy to use onshore trained algorithms to estimate offshore data is assessed and discussed by analysing the impact of distance, cardinal direction and temporal differences between training and validation stations in an onshore case study. This study aims to make concrete recommendations on the use of these MLMs in future solar resource estimation studies by identifying the impact of the external factors. In order to identify the external factors, first the optimal design of the MLMs is determined. This includes evaluating the variable importance of the input variables and an evaluation of the bias-variance tradeoff. This is followed by an onshore case study evaluating the different MLMs to identify the impact of the external factors distance, cardinal direction and temporal differences. As a result, the impact of the different external factors is reflected on the estimated offshore irradiance. Eventually this research will try to answer the following questions:

How can machine learning be used to estimate offshore solar irradiance using onshore data ?

Sub-questions:

- 1.What are the feature importance's of the input variables?

- 2.How are the MLMs affected by the bias-variance tradeoff?

- 3.What is the effect of distance on the performance of the MLMs?

- 4.What is the effect of the cardinal direction on the performance of the MLMs?

- 5.What is the effect of temporal differences on the performance of the MLMs?

By answering these questions this research will add to the understanding on how MLMs for solar resource estimation are affected by geographical and temporal factors. It provides an answer to the question whether external factors should be considered before solar resource estimations are conducted. In addition, this research serves as a guiding tool on how to asses the influence of external factors when estimating solar irradiance. As a result, this research provides recommendations for future solar resource estimation assessments in places where irradiance has not been (adequately) measured.

In section 4.2 the data used in this research is presented, followed by an introduction of the different MLMs and the bias-variance tradeoff in section 4.3. In section 4.4 the methods to answer the sub-questions are presented. In section 5 the results of the different sub-questions are presented followed by an offshore estimation in section 5.6. The results are discussed in section 6 and finally, in section 7 the conclusions of this research are presented.

4   Methods

4.1   Overview of Methods

In **sub-section 4.2** the data from the KNMI is presented and modifications to this data are explained. In **sub-section 4.3** the different MLMs are introduced. This includes an introduction of the bias-variance tradeoff and is followed by an introduction of the different MLMs. In **sub-section 4.4** the methods to evaluate the performance of the MLMs are presented for each sub-question.

4.2   Data

4.2.1   Data collection

HH	Time (Hour of day)
DD	Mean wind direction (in degrees)
FH	Hourly mean wind speed (in 0.1 m/s)
FF	Mean wind speed (in 0.1 m/s)
FX	Maximum wind gust (in 0.1 m/s)
T	Temperature (in 0.1 degrees Celsius)
TD	Dew point temperature (in 0.1 degrees Celsius)
P	Air pressure (in 0.1 hPa)
VV	Horizontal visibility (Ordinal)
N	Cloud cover (Ordinal)
U	Relative atmospheric humidity (in percent)
M	Fog (Binary)
R	Rainfall (Binary)
S	Snow (Binary)
Y	Ice formation (Binary)

Figure 2: Input variables. Source: (KNMI,2018).

The KNMI has 35 onshore weather stations and 10 offshore stations measuring meteorological data on a hourly resolution. 20 onshore stations measure solar irradiance and from these stations 15 stations are selected that have more than 60.000 measured hours without missing values in the time interval: 1 January 2000 until 31 December 2017. Furthermore, Only daytime (8:00 -20:00) is considered in this research. This results in an approximate 12.6 years of data for all onshore stations. The 15 stations are presented in table 1 on page 13. High irradiance levels are found at De Kooy, Vlissingen and Volkel, whereas low values are found for Hoogeveen and Eelde. These stations measure a total of 22 climate variables including irradiance (J/cm^2). Offshore stations measure a total of 19 climate variables (without irradiance). In total, there is a set of 15 shared variables both measured at onshore and offshore stations presented in figure 2. These variables will

be used to estimate irradiance because they are both measured at onshore and offshore stations. This public accessible data is provided by the KNMI (2018).

Station (number)	LON (East)	LAT (North)	Q mean (J/cm^2)	Q std dev. (J/cm^2)
De Bilt (260)	5.18	52.10	73.6	79.5
De Kooy (235)	4.78	52.93	79.2	85.3
Deelen (275)	5.97	52.06	74.2	79.2
Eelde (280)	6.59	53.13	72.2	78.6
Eindhoven (370)	5.38	51.45	75.9	80.5
Gilze-Rijen (350)	4.94	51.57	75.5	80.1
Hoogeveen (279)	6.57	52.75	72.5	79.2
Leeuwarden (270)	5.75	53.22	76.5	80.8
Lelystad (269)	5.52	52.46	74.3	80.7
Maastricht (380)	5.76	50.91	75.2	82.0
Rotterdam (344)	4.45	51.96	76.1	81.7
Schiphol (240)	4.79	52.32	75.8	81.8
Twente (290)	6.89	52.27	74.0	79.9
Vlissingen (310)	3.60	51.44	80.9	85.7
Volkel (375)	5.71	51.66	79.6	82.1

Table 1: Onshore stations used in this study. Source:(KNMI, 2018).

4.2.2 Data preparation

First of all, it is important to make sure there is no missing data in the training and validation datasets. Therefore, samples with at least one missing variable are removed from the dataset. Furthermore, the data is checked for anomalies to confirm the data does not contain any extreme outliers that could affect the performance of the MLMs. This is done by calculating the mean, standard deviation, maximum and minimum for all input variables. Finally, in forecasting often only daytime (e.g. 8:00-20:00) is considered as this tends to improve the forecast and thus decreases the training time. In RF and XGB, the input variables are used to split solar irradiance data based on a threshold value of a variable (sub-sections 4.3.2 and 4.3.3). Data with lower values are separated from data with values that are higher than the threshold. This mechanism works for variables with continuous data where higher values indicate higher levels of that variable. However, this mechanism does not work for the feature HH that has values ranging from 8 until 20. This variable has a sinus characteristic with higher irradiance levels at HH= 12 and lower values at HH=8 and 20. Therefore this data is transformed by multiplying the original data by the following function (Eq. 1):

$$HH = \frac{1}{2}sin\left(\frac{1}{12}\pi * (HH - 6)\right) + 1 \qquad (1)$$

This transformation ensures that RF and XGB algorithms are able to separate low and high

irradiance levels based on the time of the day. This idea is demonstrated in the figure below where in figure 3a the data is split using the untransformed dataset and in figure 3b the transformed dataset is used ensuring that lower and higher irradiance levels are separated.

(a) Split using using original data.   (b) Split using transformed data.
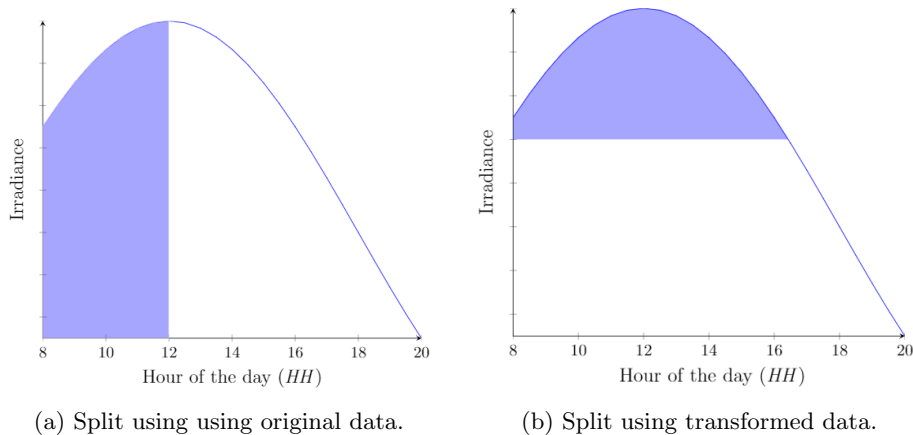
Sola and Sevilla (1997) concluded that input data normalisation with certain criteria, prior to a training process, is crucial to obtain good results as well as to improve the computation time. Therefore the input data of the ANN is normalised. The goal of normalisation is to change the values of all variables into one generic scale without a loss in information of the data. The data is normalised using the standard error (Eq. 2) where x is the original value of the variable, μ the mean of variable x, and σ the standard deviation of variable x. The binary variables are not normalised.

$$StandardError = \frac{x - \mu}{\sigma} \tag{2}$$

4.3 Machine Learning

4.3.1 Bias-variance tradeoff

MLMs can be designed in a very shallow or extremely complex manner. Training of a MLM improves the understanding between the variables and their correlations to calculate the desired output(Fortmann-Roe, 2012). However, increasing the complexity does not necessarily improve the result. An extensively trained MLM with a high model complexity has the tendency to overfit. As more parameters are added to the model, the model complexity increases which results in a high variance. On the other hand, when a low complexity MLM is trained, the algorithm is not able to identify the important relations between the variables (Goodfellow, 2016). This will result in a high bias but a lower variance called underfitting. This tradeoff, visualised in figure 4 is important
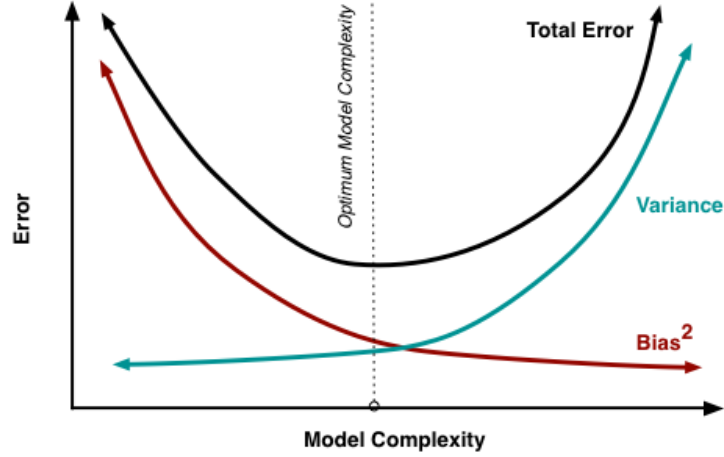
Figure 4: Bias-variance tradeoff. Source: (Fortmann-Roe, 2012).

considering the performance of MLMs. In this research, the aim is to minimise the bias, referred to as the 'absolute error', without significantly increasing the variance, referred to as the 'relative error'. In **sub-section 4.4.2** the calculations for the absolute and relative errors will be explained in further detail.

4.3.2 Random Forest (RF)

Rf is originally developed by Breimann in 2001. In RF a number of decision trees is generated with for every tree a set of n layers. In every n^{th} layer there are 2^n decision nodes with n=0 for the first layer. Every decision node has its own characteristic variable constraints and based on these constraints, the node will pass a true or false to the node y in the next layer $(n + 1)$. In the last layer (leaf layer), for regression this will result in an estimation of the target value based on the average of all samples reaching that node (Breiman, 2001). In RF multiple decisions trees are generated. Every tree is trained using a random subset of the training data. The same training data can be selected by different trees in the forest, this process is called bagging. Figure 5 visualises a shallow decision tree with 2 layers. In this example the first split is based on the variable relative humidity (U). In the second layer both splits are based on the time of the day (HH). This results in 4 different predictions for irradiance. If this tree predicts the irradiance of a sample with $U= 80$ and $HH =0.9$, this will result in an estimated irradiance of 65 J/cm^2. The maximum number of variables to consider at a split is also important. If this for example is set to 5 variables, for every split only 5 out of 15 variables are randomly considered to make the best split. Lower values reduce the relative error but increases the absolute error. In this research the optimal number of trees, layers and number of variables to consider at every split are determined

to minimise the Bias-variance tradeoff. The RandomForestRegressor from the SKlearn library is used to perform this analysis. The Python script of this analysis can be found in appendix section A.1.1.
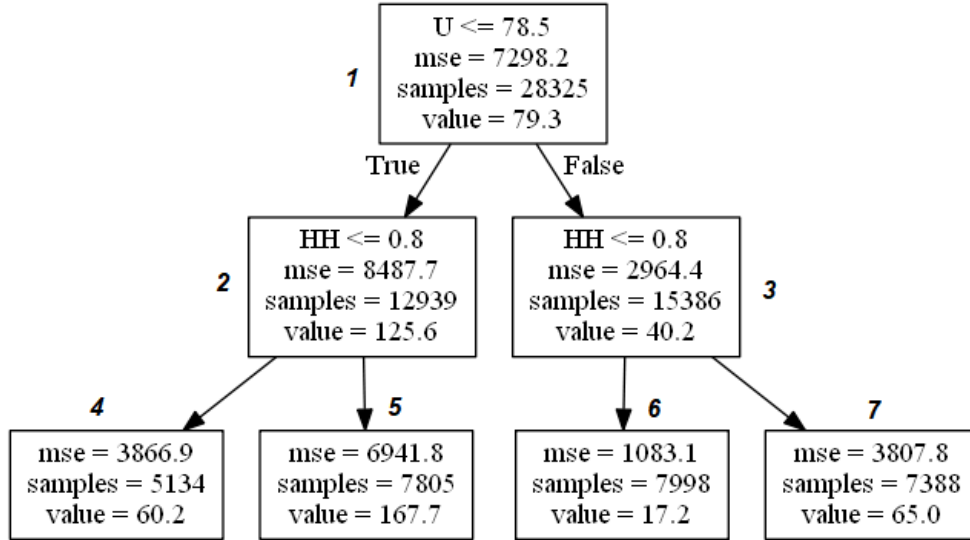
Figure 5: Example of a shallow decision tree.

4.3.3 Extreme Gradient Boosting (XGB)

The XGB algorithm is originally developed by Friedman in 2001. The main difference between XGB and RF is that the former generates one tree at a time to improve the performance of the previous tree wheras the latter trains each tree independently (Voyant et al., 2017). The first tree uses the deviation of the mean as input residual, and a second tree uses the residuals of the first tree to decrease the errors of the first tree (Fan et al. 2018). This process is repeated a number of times based on the stopping criteria. In figure 6 an example is presented for a small XGB algorithm with 3 trees. Table 2 presents the calculations used in this XGB algorithm. Q is the targeted irradiance value in J/cm^2. $H0$ represent the estimated irradiance based on the mean of Q. $R0$ is the residual used as input for the first tree and is calculated by $Q - H0$. $P1$ is the prediction of the first tree and is calculated by averaging the residuals that end at up at the same leaf node. For the left node of the first tree: $P1 = (-106.8 - 39.8 - 37.8)/3 = -61.4$ (Figure 6). The estimated irradiance of the first tree ($H1$) is than computed by the following formula: $H0 + (P1 * l)$ where l is the learning rate, a parameter that controls how fast the algorithm learns. Subsequently, this process is repeated and $R1$ is calculated by $Q - H1$ and used as input for the second tree. This process is repeated indicated by the number of trees. In this research the optimal number of layers, trees and the learning rate are determined to minimise the Bias-Variance tradeoff. The GradientBoostingRegressor from the SKlearn library is used to perform this analysis. The Python

16

script of this analysis is fairly similar to the RF script and can be found in appendix section A.1.2.

Q	H0	R0	P1	H1	R1	P2	H2
9	115.8	-106.8	-61.4	109.6	-100.6	-55.3	104.1
76	115.8	-39.8	-61.4	109.6	-33.6	-55.3	104.1
300	115.8	184.3	184.3	134.2	165.8	165.8	150.8
78	115.8	-37.8	-61.4	109.6	-31..6	-55.3	104.1

Table 2: Example of calculations behind XGB.
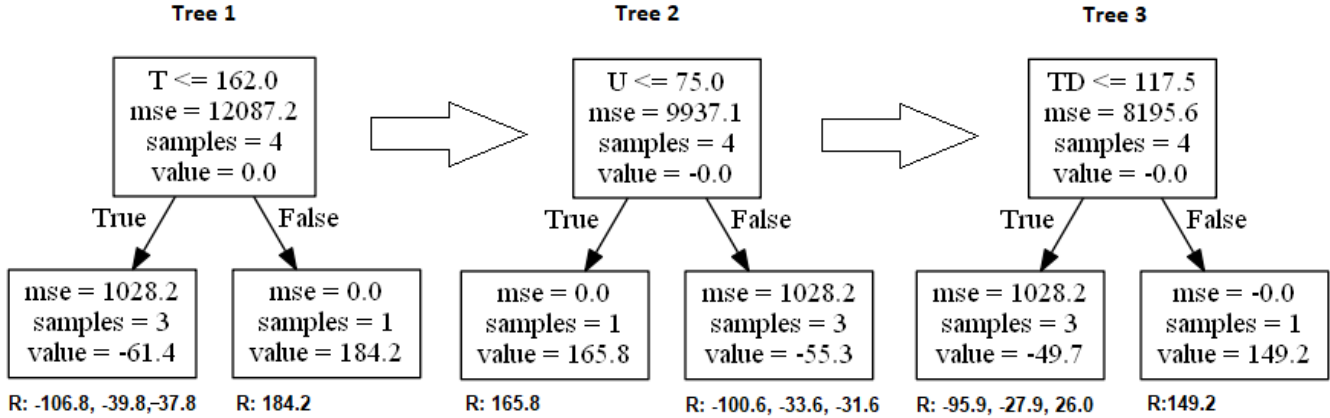
Figure 6: Example of XGB trees.

4.3.4 Artificial Neural Networks (ANN)

ANN's consist of one input layer, a number of hidden layers in between and one output layer. If the input layer has N nodes, the output of a node in the first layer is given by Eq. 3, where z is the output of the node to the next layer, w_i represents the weights multiplied by the x_i outputs of the nodes in the previous layer and b is the bias of the node. This output is summed for all the nodes of the previous layer and multiplied by the specified activation function σ. An example of an activation function is the sigmoid function (Eq.4) that converts the output of the node in to a non-linear output (Rehmann, 2008).

$$z = \sigma \sum_{i=1}^{N} (w_i * x_i) + b \tag{3}$$

$$\sigma = \frac{e^x}{e^x + 1} \tag{4}$$

In the output layer, the output $\hat{y}$ is compared to the actual value y with a cost function. In this research the Mean Squared Error (MSE, Eq.5) is used as the cost function. In the next step the weights and biases in the network are adjusted using the error computed in the cost function. The

number of epochs indicates how often the same training data is fed to the network. The batch size indicates the number of samples before weights and biases are updated. The ultimate design of the ANN determines the performance related to the bias-variance tradeoff (Jain, 1996). In this research the optimal number of layers, nodes, epochs and batch size are determined. In addition, the best performing learning rate, activation function and optimisation function are determined. In figure 7 on page 18 an example of a network is visualised. In the input layer the X variables correspond to the the different climate variables introduced in figure 2 on page 12. Between the input and output layer is a number of hidden layers, and at the end there is one output node with the irradiance prediction. The Keras library of the Tensorflow package is used for this analysis. Keras is a high-level Application Programming Interface (API) to build and train deep learning models. It's used for fast prototyping, advanced research, and production (Tensorflow,2019). The Python script can be found in appendix section A.1.3.
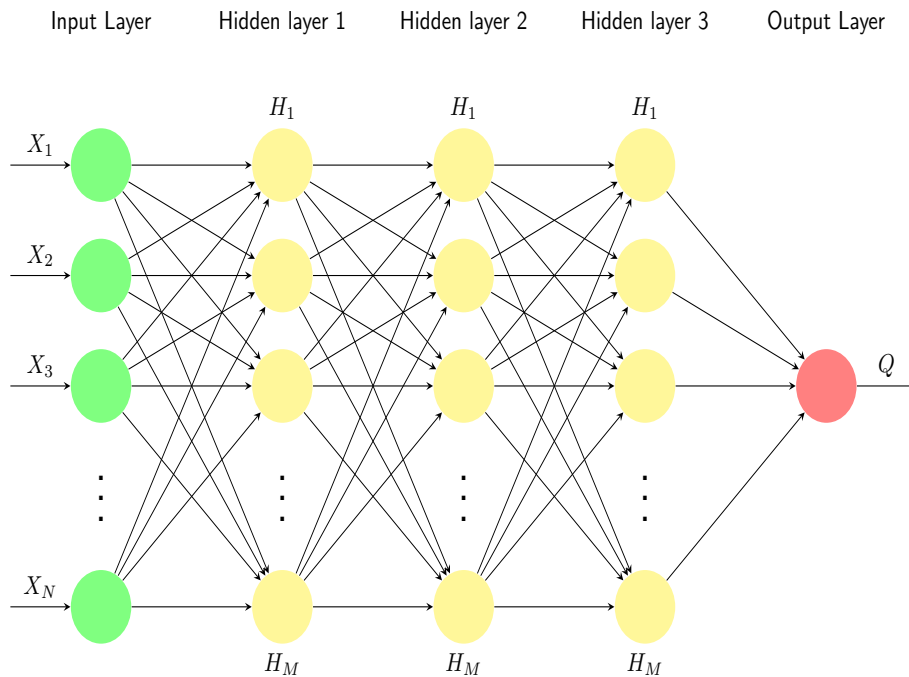
Figure 7: Example of a design of the ANN.

4.4 Performance Evaluation

4.4.1 Feature Importance

To determine the importance of the variables used to predict irradiance, the MLMs RF and XGB are used. Next to the predictive power of these two MLMs they are often used to determine the feature importance of variables (Qi,2012 & Saeys, 2008 & Ma et al., 2017 & Zheng et al.,2017). In RF and XGB regression the feature importance is calculated using the mean Mean Decrease in Impurity (MDI). In this research the MSE (Eq.5) is used as impurity measure. The MDI of one node is calculated using Eq. 6, where MDI_B is the impurity of the base node, I_B is the original MSE of the base node multiplied by the fraction of samples in the bases node N_B. I_L and I_R are the MSE of the left and right splitting nodes multiplied by the fractions N_L and N_R representing the share of samples reaching these particular nodes.

$$MSE = \frac{1}{N} * \sum_{i=1}^{N} \left(\hat{y}(i) - y(i) \right)^2 \tag{5}$$

$$MDI_B = (I_B * N_B) - (I_L * N_L) - (I_R * N_R) \tag{6}$$

In the context of random trees in RF and XGB, the feature importance of variable X is calculated by summing all MDI's of the nodes where feature X is used to split the data divided by the total MDI of all the nodes in the tree. The next step is to average the feature importance over all the trees. To answer the first sub-question the results of the RF and XGB are compared to make conclusions about the feature importance.

As an example how the feature importance for one tree is derived reconsider figure 5 from section 4.3.2. The feature importance of U and HH is calculated using Equations 7 until 12. N_{tot} is the total number of samples in the tree, N_x is the number of samples in node x, MSE_x is the mean squared error of node x and I_U and I_H are the resulting feature importances.
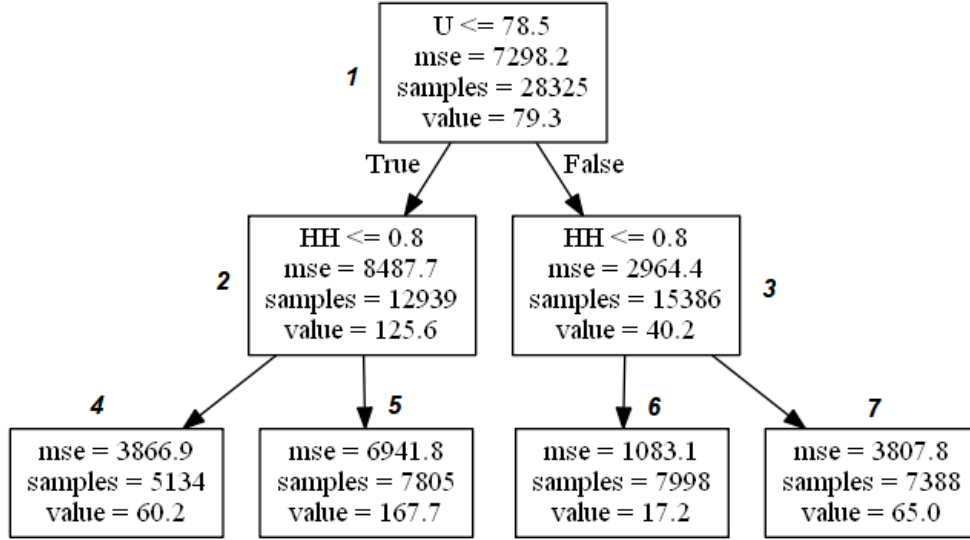
Figure 8: Example of a shallow decision tree.

$$MDI_U = (MSE_1 * \frac{N_1}{N_{tot}}) - (MSE_2 * \frac{N_2}{N_{tot}}) - (MSE_3 * \frac{N_3}{N_{tot}}) \tag{7}$$

$$MDI_{HH_2} = (MSE_2 * \frac{N_2}{N_{tot}}) - (MSE_4 * \frac{N_4}{N_{tot}}) - (MSE_5 * \frac{N_5}{N_{tot}}) \tag{8}$$

$$MDI_{HH_3} = (MSE_3 * \frac{N_3}{N_{tot}}) - (MSE_6 * \frac{N_6}{N_{tot}}) - (MSE_7 * \frac{N_7}{N_{tot}}) \tag{9}$$

$$MDI_H = MDI_{HH_2} + MDI_{HH_3} \tag{10}$$

$$MDI_{tot} = MDI_H + MDI_U \tag{11}$$

$$I_U = \frac{MDI_U}{MDI_{tot}} \quad \& \quad I_H = \frac{MDI_H}{MDI_{tot}} \tag{12}$$

When evaluating the variable importance, it is important to take into account the (anti-) correlation between variables: When variable X and Y are highly correlated and both have a high correlation with irradiance, both variables have a high probability to be selected to split irradiance data. When variable X is used to split the data, this significantly reduces the importance of variable Y, since the impurity variable Y can remove has already been removed by variable X. Therefore, it is important to identify the (anti-)correlations between the variables. The Pearson correlation ($\rho_{X,Y}$) between variable X and Y is calculated using equation 13 where $\overline{X}$ and $\overline{Y}$ are the mean values of X an Y respectively.

$$\rho_{X,Y} = \frac{\sum_{i=1}^{N}(X_i - \overline{X})(Y_i - \overline{Y})}{\sqrt{\sum_{i=1}^{N}(X_i - \overline{X})^2(Y_i - \overline{Y})^2}} \tag{13}$$

4.4.2 Bias-variance tradeoff

Let us consider a fictional station A. First the data of station A is split into a training and a validation dataset. Subsequently, the MLM is trained on the training set and validated on the validation set. The MLM calculates irradiance levels of the validation set and compares this to actual irradiance levels of the validation set resulting in the absolute error of station A ($A_{A,A}$). This error is calculated using three commonly used metrics (Eq.14-16) (Voyant et al., 2017). With $\hat{y}$ being the calculated irradiance, y the actual irradiance, $\overline{y}$ the mean of y and N the number of observations.

$$MAE = \frac{1}{N} * \sum_{i=1}^{N} |\hat{y}(i) - y(i)| \tag{14}$$

$$RMSE = \sqrt{\frac{1}{N} * \sum_{i=1}^{N} \left(\hat{y}(i) - y(i)\right)^2} \tag{15}$$

$$nRMSE = \frac{RMSE}{\overline{y}} \tag{16}$$

The next step is to use the trained algorithm of station A to calculate the irradiance at another fictional station B. This calculated irradiance data is compared to actual irradiance levels at station B resulting in the **absolute error** $A_{A,B}$. To correct for the training error of station A, $A_{A,B}$ is divided by $A_{A,A}$ reflecting the performance of estimating B based on model trained at A, also called the **relative error** $R_{A,B}$ (Eq. 17).

$$\begin{bmatrix} A_{A,A} & A_{A,B} \\ A_{B,A} & A_{B,B} \end{bmatrix} / \begin{bmatrix} A_{A,A} \\ A_{B,B} \end{bmatrix} = \begin{bmatrix} 1 & R_{A,B} \\ R_{B,A} & 1 \end{bmatrix} \tag{17}$$

In this research 15 onshore stations are used for the analysis. This results in an absolute error matrix X (Eq. 18) and a relative error matrix Y (Eq. 19) that contain 15 x 15 = 225 errors for all combinations between the stations with 1's on the diagonal for matrix Y:

$$X = \begin{bmatrix} A_{1,1} & \dots & A_{1,15} \\ \vdots & \ddots & \vdots \\ A_{15,1} & \dots & A_{15,15} \end{bmatrix} \tag{18}$$

$$Y = \begin{bmatrix} 1 & \dots & R_{1,15} \\ \vdots & \ddots & \vdots \\ R_{15,1} & \dots & 1 \end{bmatrix} \tag{19}$$

To answer the second sub-question, these absolute and relative errors are computed for different MLMs by changing the hyperparameters introduced in section 4.3. The optimal configuration of hyperparameters is determined by minimising the product mean(X) * mean(Y), thereby minimising the bias-variance tradeoff (Eq.20). The optimal design is used in the remaining part of this research. If there is a small difference between two hyperparameter configurations but a significant increase in computation time, the configuration with the lowest computation time is used. In order to put the results of the MLMs in perspective, the results are compared to a reference linear regression model. The LinearRegression model from the SKlearn library is used to perform this analysis.

$$\textbf{\textit{Minimze:}} \quad XY = mean(X) * mean(Y) \tag{20}$$

4.4.3 Distance and cardinal performance

To assess the effect of distance between the 15 considered stations on the performance of the MLMs, a distance matrix X_D (Eq. 21) is created that contains all distances D between the 15 stations with zeros on the diagonal. To determine the distance performance matrix Y is plotted against X_D.

$$X_D = \begin{bmatrix} 0 & \dots & D_{1,15} \\ \vdots & \ddots & \vdots \\ D_{15,1} & \dots & 0 \end{bmatrix} \tag{21}$$

Similar to the distance performance, here a matrix X_C (Eq. 22) is created containing all the cardinal directions between the stations (E= 0°, N= 90°, W= 180°, S= 270°). For example: station B is north-west of station A resulting in a value for $C_{A,B} = 45°$. Matrix Y is plotted against matrix X_C to detect a possible relation. The results will be visualised using polar plots. The different MLMs are compared using these plots to make conclusions on the effect of the cardinal direction.

$$X_C = \begin{bmatrix} 0 & \dots & C_{1,15} \\ \vdots & \ddots & \vdots \\ C_{15,1} & \dots & 0 \end{bmatrix} \tag{22}$$

4.4.4 Temporal performance

Offshore data is measured from 2010 until 2018 and onshore training data is used from 2000 until 2018. This results in a temporal difference between training and validation data. In this analysis 150.000 training and 40.00 validation samples are randomly selected from all onshore stations (Table 3). To answer the fifth sub-question and evaluate the effect of this temporal difference between training and validation data two assessments are performed:
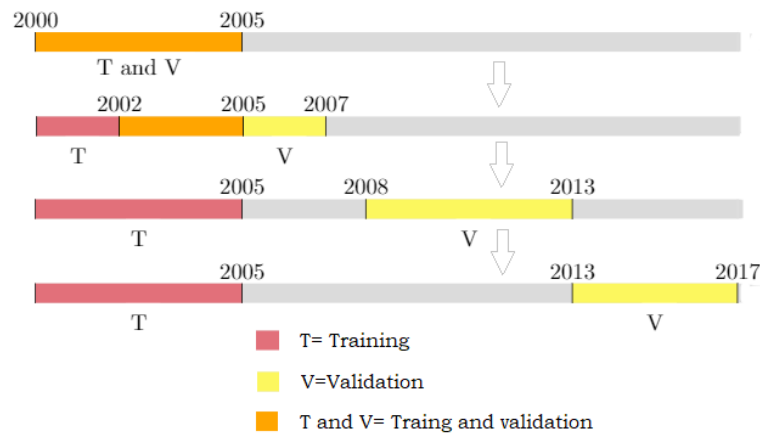
Figure 9: Temporal effect: fixed training interval.

- How is the validation accuracy affected by **a changing validation interval with a fixed training interval?** In figure 9 the data is trained in the period between 2000 and 2005 for a 5 year time interval. The validation interval is shifted towards the right side of the timeline with a delta t of 1 year. This results in 14 validation errors. The relative errors are calculated by dividing the the 14 validation errors by the validation error of the reference training interval (2000-2005).
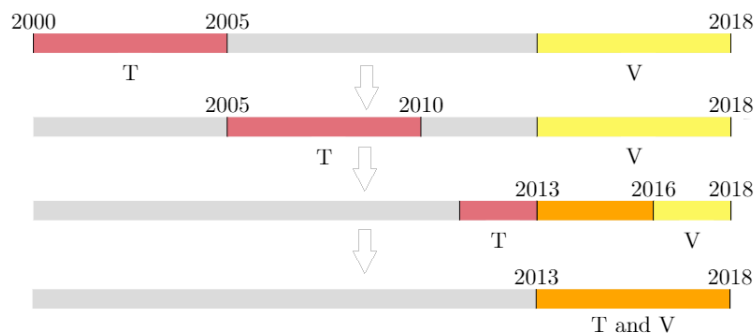
Figure 10: Temporal effect: fixed validation interval.

- How is the validation accuracy affected by **a changing training interval with a fixed validation interval?** In figure 10 the data is validated in the period between 2013 and 2018 for a 5 year time interval. The training interval is shifted towards the right side of the timeline with a delta t of 1 year. This results in 14 validation errors. The relative errors are calculated by dividing the 14 validation errors by the validation error of the reference validation interval (2013-2018).

Validation Interval	Training samples	Validation samples
5 Years	150.000	40.000

Table 3: Number of samples.

4.4.5 Offshore estimation

Finally, an offshore estimation is conducted after answering the questions addressed. Onshore stations will be selected for the estimation of offshore irradiance based on the findings of this study. The results of this estimation are compared to those of onshore irradiance in order to draw conclusions on offshore irradiance levels. Furthermore, the results are reflected with respect to the influence of the external factors.

5 Results

5.1 Feature Importance

To answer the first sub-question the feature importance is discussed for the RF and XGB algorithms. Furthermore, the correlation between the input variables is discussed. The last part gives a conclusion regarding the feature importance.

5.1.1 Random Forest

The variables importance for the RF is calculated by generating 1 tree with K Layers for all 15 onshore training stations taking the average of the trees as the feature importance. The number of trees is set at 1 per station because trees in the RF algorithm do not vary significantly and therefore will not affect the outcome. From figure 11 it can be concluded that relative humidity (U) has the highest feature importance followed by the hour of the day (HH) and temperature (T). This importance is lower for K=20 and the importance of temperature, cloud cover (N) and wind direction (DD) increase. According to these results it can be concluded that the RF algorithm is strongly influenced by relative humidity.
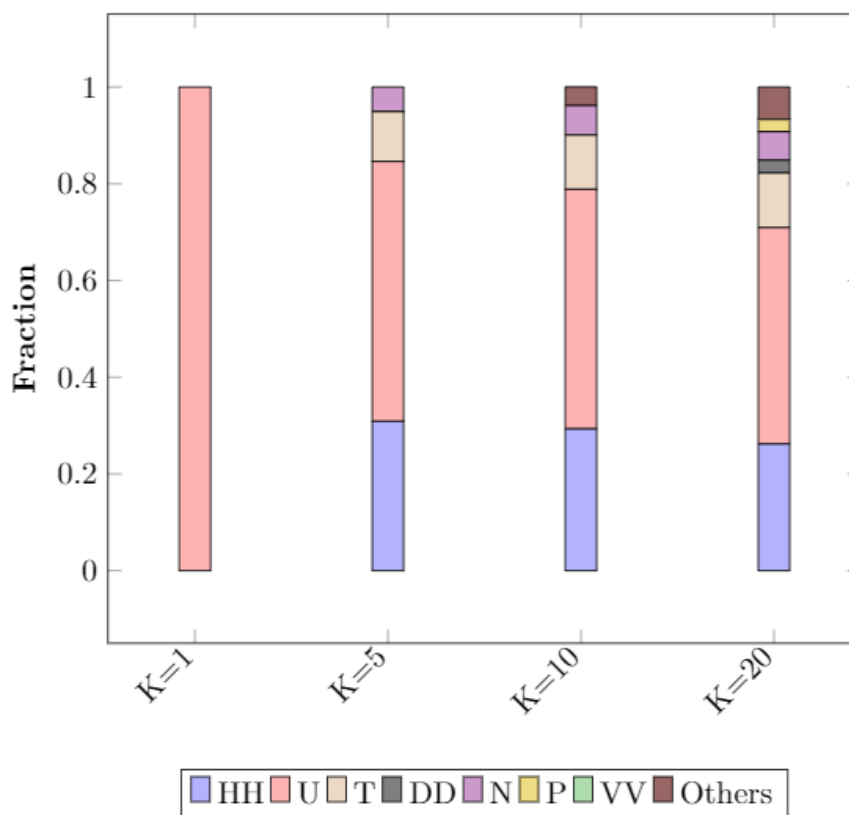
Figure 11: Feature importance of RF for different number of layers (K).

5.1.2 Extreme Gradient Boosting
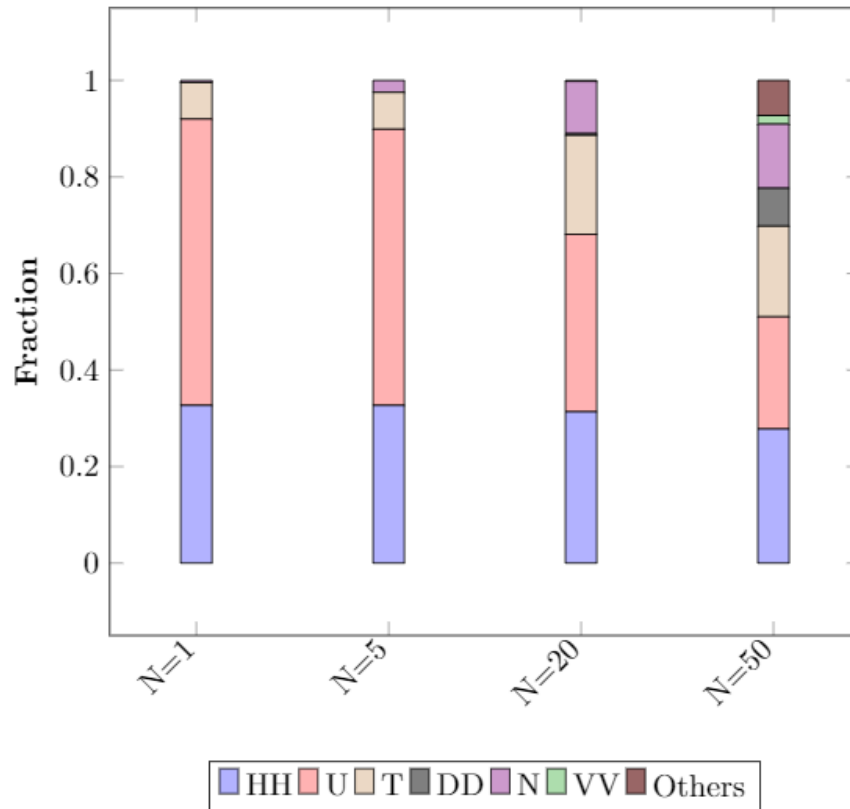
Figure 12: Feature importance of XGB for different number of trees (N).

The feature importance for the XGB algorithm is calculated by generating a number of trees (N) for a fixed number of 3 layers using a learning rate of 0.1. Figure 12 shows the results for this assessment. From these results it can be concluded that the importance of U decreases strongly with an increasing number of trees. Furthermore it can be denoted that the variables T and N have a significant share for N=50.

5.1.3 Comparison RF and XGB
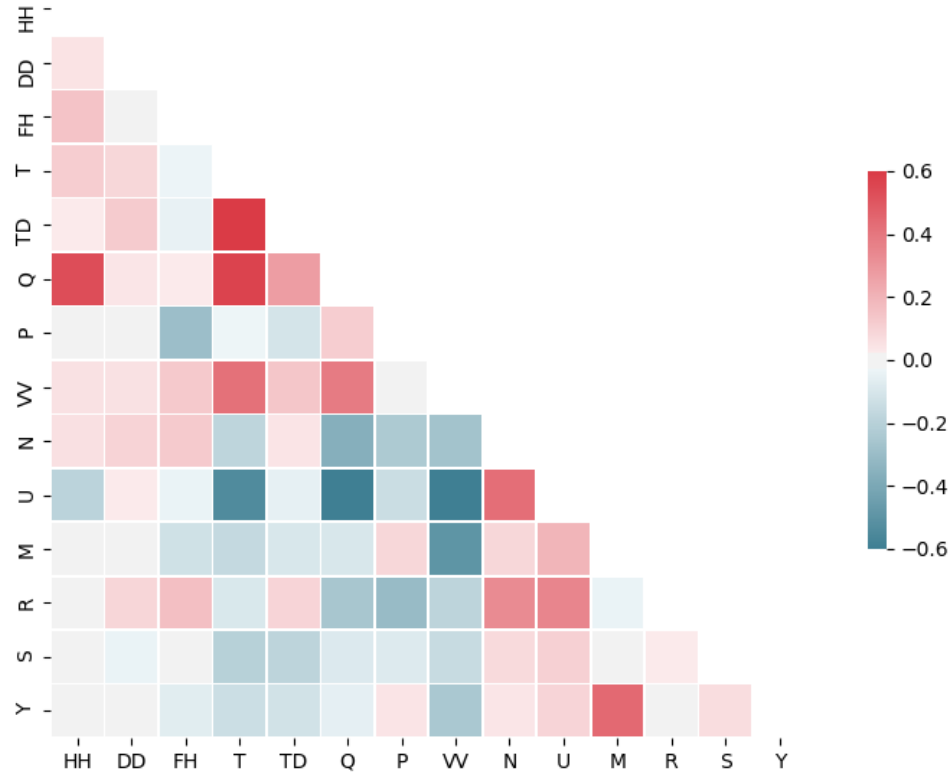
Figure 13: Pearson correlation between used variables.

Figure 13 shows that irradiance is correlated with the variables daytime (HH) , temperature (T), dew point temperature (TD) and horizontal visibility (VV). Furthermore irradiance (Q) has a strong anti-correlation with relative humidity (U). U is strongly anti-correlated with T and VV which indicates that the variable importance of T and VV is significantly reduced by U. If the variable U would not be used as input variable in RF and XGB, this would result in a higher variable importance of T and VV. This is important to consider when making conclusions about feature importance to predict solar irradiance. The RF and XGB algorithm are strongly influenced by the variables U and HH but it is important to take into account the correlations between variables to make conclusions about the actual feature importance to estimate solar irradiance. Compared to the results from RF, other variables such as T and N have a significant larger share in XGB. As discussed in section 4.3.2 and 4.3.3, the XGB algorithm uses the residuals of the precedent tree as input for the next tree, whereas the RF algorithm takes a random subset of

the original data for every tree. This explains the different outcome of the two MLMs regarding the feature importance. In the RF algorithm, the Pearson correlation between Q and the other variables is constant for all trees in the forest. In the contrary, XGB uses residuals of the precedent tree and therefore the correlation between the residuals of Q and other variables changes when more trees are added to the model. When U is used to decrease the impurity in the first tree, this in turn results in an information loss for U in the next tree. In contrast, N is not used in the first tree, therefore there is no information loss and the correlation between N and the residuals of Q remains constant in the first tree. The difference in feature importance between RF and XGB clearly shows that the importance of a variable depends on the MLM and its design. The advantage of calculating the feature importance is that it provides a clarification how the MLM derives its results. However, the results should not be used to make conclusions about the actual relation between the irradiance and other climate variables. Instead, it should be interpreted as a clarification how RF and XGB derive their results. Since the aim of this research is to compare the performance of different MLMs, it is important that all MLMs use the same set of variables therefore all variables are used in the remaining of this analysis.

5.2 Design of the MLMs

In this section the optimal size of the RF, XGB and ANN algorithms are determined by minimising the bias-variance tradeoff. This is followed by a comparison of the MLMs related to the bias-variance tradeoff.

5.2.1 Random Forest

Table 4 shows the absolute and relative errors for different number of trees and layers. Each number in the table represent an average performance of all 225 combinations between stations. It can be concluded that the lowest absolute errors are achieved by a model with 15 layers and 100 trees indicating this forest has the highest absolute accuracy. However, the relative error of this forest is significantly higher compared to a forest with 10 layers. A relative error of 1.5 indicates that on average the error increases by 50% when a trained model is validated at another station. This means overfitting occurs using a model with 15 layers. On the other hand, using a shallow forest with 5 layers results in higher absolute errors. High absolute errors indicate that the RF is too shallow and therefore unable to accurately predict irradiance. By multiplying the absolute and relative errors the lowest resulting values can be found for (N=50, K=10) and (N=100, K=10). Computation time is significantly larger for N=100, therefore N is set at 50. This RF size is used in the remaining part of this research.

Absolute	N=5			N=50			N=100		
	MAE	*RMSE*	*nRMSE*	*MAE*	*RMSE*	*nRMSE*	*MAE*	*RMSE*	*nRMSE*
K=5	27.04	38.86	0.51	26.80	38.44	0.51	26.80	38.43	0.51
K=10	23.22	34.45	0.45	22.67	33.49	0.442	22.81	33.66	0.44
K=15	23.45	35.14	0.46	22.31	33.16	0.44	22.25	33.06	0.44
Relative	N=5			N=50			N=100		
	MAE	*RMSE*	*nRMSE*	*MAE*	*RMSE*	*nRMSE*	*MAE*	*RMSE*	*nRMSE*
K=5	1.05	1.06	1.06	1.05	1.06	1.06	1.05	1.06	1.06
K=10	1.15	1.15	1.15	1.15	1.16	1.16	1.15	1.16	1.16
K=15	1.50	1.44	1.44	1.53	1.49	1.49	1.53	1.50	1.50

Table 4: Absolute and relative errors for different sized number of trees (N) and number of layers (K) in RF.

The maximum number of features (F) to consider at a split is also determined and the result are presented in table 9 in appendix section A.2. From this table it can be concluded that the absolute error remains the same for F=10 and F=15 but the relative error decrease slightly. Therefore F=10 is used in the remaining of this research.

5.2.2 Extreme Gradient Boosting

Instead of using deep decision trees in RF, XGB generates many shallow trees in a sequential manner, meaning it aims to improve the previous tree. The most important difference between RF and XGB which can be identified in the table 5, is that relative errors are generally lower. XGB has a lower tendency to overfit since it uses the residuals as input for the next tree. This shows that the performance of XGB can be optimised without having a large effect of overfitting which is the case for the RF algorithm. The optimal parameters for the XGB algorithm are 100 trees with a learning rate of 0.10 and 200 trees with a learning rate of 0.05. The difference between (N=100,l=0.10) and (N=200,l=0.05) is relatively small. Considering computation time, N is set at 100 and l at 0.10. Furthermore the optimal number of layers is found to be relatively shallow (table 10, appendix section A.2) at K=4 layers. K=3 layers results in underfitting whereas K=5 layers results in overfitting.

Absolute	N=50			N=100			N=200		
	MAE	*RMSE*	*nRMSE*	*MAE*	*RMSE*	*nRMSE*	*MAE*	*RMSE*	nRMSE
l=0.05	26.34	35.80	0.472	23.51	33.73	0.445	22.92	33.11	0.436
l=0.10	23.52	33.76	0.445	22.93	33.12	0.437	22.63	32.76	0.432
l=0.15	23.16	33.39	0.441	22.78	32.95	0.434	22.59	32.69	0.431
Relative	N=50			N=100			N=200		
	MAE	*RMSE*	*nRMSE*	*MAE*	*RMSE*	*nRMSE*	*MAE*	*RMSE*	*nRMSE*
l=0.05	1.055	1.067	1.066	1.077	1.086	1.085	1.092	1.099	1.099
l=0.10	1.077	1.086	1.085	1.092	1.099	1.099	1.111	1.116	1.115
l=0.15	1.085	1.093	1.092	1.102	1.107	1.107	1.126	1.129	1.129

Table 5: Absolute and relative errors for different number of trees (N) and learning rates (l) for XGB.

5.2.3   Artificial Neural Networks

ANN can be extremely complex or very shallow and compared to RF and XGB more hyperparameters can be adjusted. Due to time constraints the hyperparameter optimisation of the network is based on training of a network using only data of station De Bilt which is located in the center of the country. Validation is done for all other onshore stations. After the hyperparameter optimisation, the obtained parameters are used to train all onshore stations similar to the RF and XGB analysis. It must be denoted that hyperparameters can interact and therefore the sequence of tuning can vary.

- **Batch size and number of epochs**: The batch size is the number of samples that is fed to the network before the weights and biases are updated. The number of epochs indicates how often the same training data is used by the network for training. This network is trained using 2 hidden layers with both 32 nodes. From table 6 it can be concluded that a network with Batch size of 20 and 100 epochs has the lowest combined absolute and relative errors.

Absolute	E=10			E=50			E=100		
	MAE	*RMSE*	*nRMSE*	*MAE*	*RMSE*	*nRMSE*	*MAE*	*RMSE*	nRMSE
B=10	22.96	33.20	0.438	21.88	31.92	0.420	21.48	31.67	0.417
B=20	24.08	34.26	0.451	22.03	32.00	0.421	21.62	31.54	0.415
B=60	28.30	41.17	0.543	22.62	32.42	0.427	21.96	31.81	0.419
B=100	37.49	57.41	0.757	23.06	32.76	0.432	21.87	31.83	0.420
Relative	E=10			E=50			E=100		
	MAE	*RMSE*	*nRMSE*	*MAE*	*RMSE*	*nRMSE*	*MAE*	*RMSE*	*nRMSE*
B=10	1.075	1.074	1.034	1.094	1.092	1.051	1.096	1.091	1.05
B=20	1.069	1.070	1.030	1.091	1.087	1.047	1.086	1.083	1.043
B=60	1.062	1.058	1.020	1.081	1.083	1.043	1.086	1.085	1.045
B=100	1.061	1.053	1.015	1.075	1.079	1.040	1.088	1.086	1.045

Table 6: Absolute and relative errors for different Batch size (B) and number of Epochs (E).

- **Optimiser:** The Keras library contains a set of different optimiser algorithms that are used to minimise the loss function. The lowest combined absolute and relative errors are found for the RMSprop algorithm. Results for different optimiser algorithms can be found in table 11 in appendix section A.2.

- **Learning rate:** The learning rate controls how much the weights are adjusted after a batch is trained. From table 12 in appendix section A.2 it can be concluded that a learning rate of 0.005 results in the optimal performance.

- **Activation function:** The activation function converts the sum of the inputs in a node to a non-linear output signal. Without the activation function the output of a node would be a linear function which would limit the complexity of the network. From table 13 in appendix section A.2 it can be concluded that the Sigmoid and Relu function show similar results. For this analysis the Sigmoid function is used since the relative errors are slightly lower.

- **Number of layers and nodes:** Table 7 shows the results for the design of the network with the number of hidden layers and number of nodes per layer. From the table, it can be concluded that a ANN with 3 layers each containing 16 nodes results in the lowest combined error.

Absolute	**L=1**			**L=2**			**L=3**		
	MAE	*RMSE*	*nRMSE*	*MAE*	*RMSE*	*nRMSE*	*MAE*	*RMSE*	*nRMSE*
N=16	23.11	33.15	0.437	21.68	31.75	0.418	21.26	31.48	0.415
N=32	23.17	32.95	0.434	21.46	31.52	0.415	21.26	31.88	0.420
N=64	23.11	32.96	0.434	21.51	31.53	0.415	21.77	32.39	0.427
Relative	**L=1**			**L=2**			**L=3**		
	MAE	*RMSE*	*nRMSE*	*MAE*	*RMSE*	*nRMSE*	*MAE*	*RMSE*	*nRMSE*
N=16	1.086	1.088	1.047	1.095	1.090	1.05	1.096	1.088	1.048
N=32	1.082	1.086	1.046	1.096	1.088	1.048	1.097	1.091	1.050
N=64	1.084	1.088	1.048	1.10	1.093	1.052	1.097	1.093	1.053

Table 7: Absolute and relative errors for different number of layers (L) and number of nodes (N) per layer.

5.2.4 Comparison of the MLMs

Considering the bias-variance tradeoff the results of the different MLMs discussed in the previous sections are compared in one graph. Figure 14 summarises the results for different sized MLMs with corresponding relative and absolute errors. Each point in the graph represents a different configuration of hyperparameters. ANN has more configurations of hyperparameters compared to XGB and RF and therefore has more data points. The black circle represent the performance of a reference linear regression model. The closer a point is to the left corner of the graph, the higher the performance related to the bias-variance tradeoff. From figure 14 it can be concluded that all MLMs have significant lower absolute errors compared to the linear regression model. Furthermore, figure 14a shows that ANN has the highest performance related to the bias-variance tradeoff, reaching a mean absolute value of around $21.5 J/cm^2$ with a mean relative error of around 1.10, indicating the error increases by 10% when a trained model is validated at another station. XGB shows slightly higher absolute errors around $22.5 J/cm^2$ with a relative error of 1.10, indicating that ANN outperforms XGB related to the bias-variance tradeoff. RF has the lowest performance regarding the Bias-variance tradeoff reaching absolute errors around $22.7 J/cm^2$ with a relative

error of 1.15. Results for RMSE and nRMSE are comparable with the results of MAE. From the results it can be concluded that the ANN has the highest performance related to the bias-variance tradeoff. Therefore, it is recommended to use the ANN to estimate offshore irradiance. The resulting absolute and relative errors between the 15 stations of the optimal designed MLMS can be found in appendix section A.3.

a: MAE.

b: RMSE.
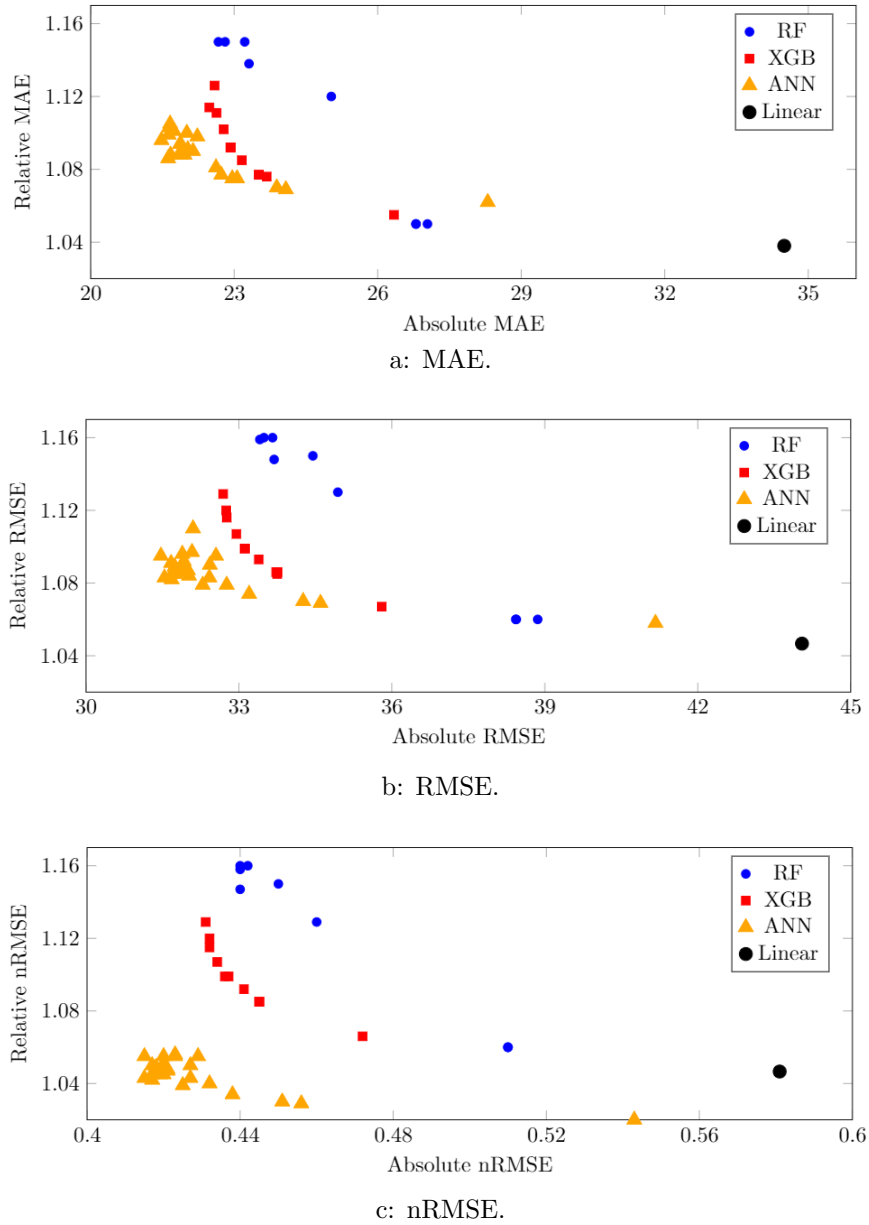
c: nRMSE.

Figure 14: Bias-variance tradeoff results for MAE (a), RMSE (b) and nRMSE(c).

5.3 Distance performance

To answer the third sub-question the relative errors are plotted against the distance between training and validation stations. This shows to what extent the error increases with distance. The results for MAE are presented in figure 15. Results for RMSE and nRMSE are comparable and can be found in appendix section A.4. The figure shows the relative MAE for different distance intervals and the standard deviations. From figure 15 there are several conclusions. For all MLMs, there is a clear increase of the relative error when the distance between training and validation station increases. RF has an average relative error around 1.10 in the interval 0-40 km and an average relative error around 1.20 in the interval 240-280 km. XGB has an average relative error around 1.05 in the interval 0-40 km and an average relative error around 1.10 in the interval 240-280 km. ANN shows slightly lower errors compared to XGB. Overall there is a clear increase of the relative error with larger distances. Furthermore it can be denoted that the standard deviation increases for larger distances. This indicates that there is an increasing uncertainty in the accuracy of the MLMs for larger distances. Based on these results there is a clear indication that the accuracy of MLMs is affected by the distance between training and validation stations. Therefore, this external factor should be taken into account for the offshore estimation.
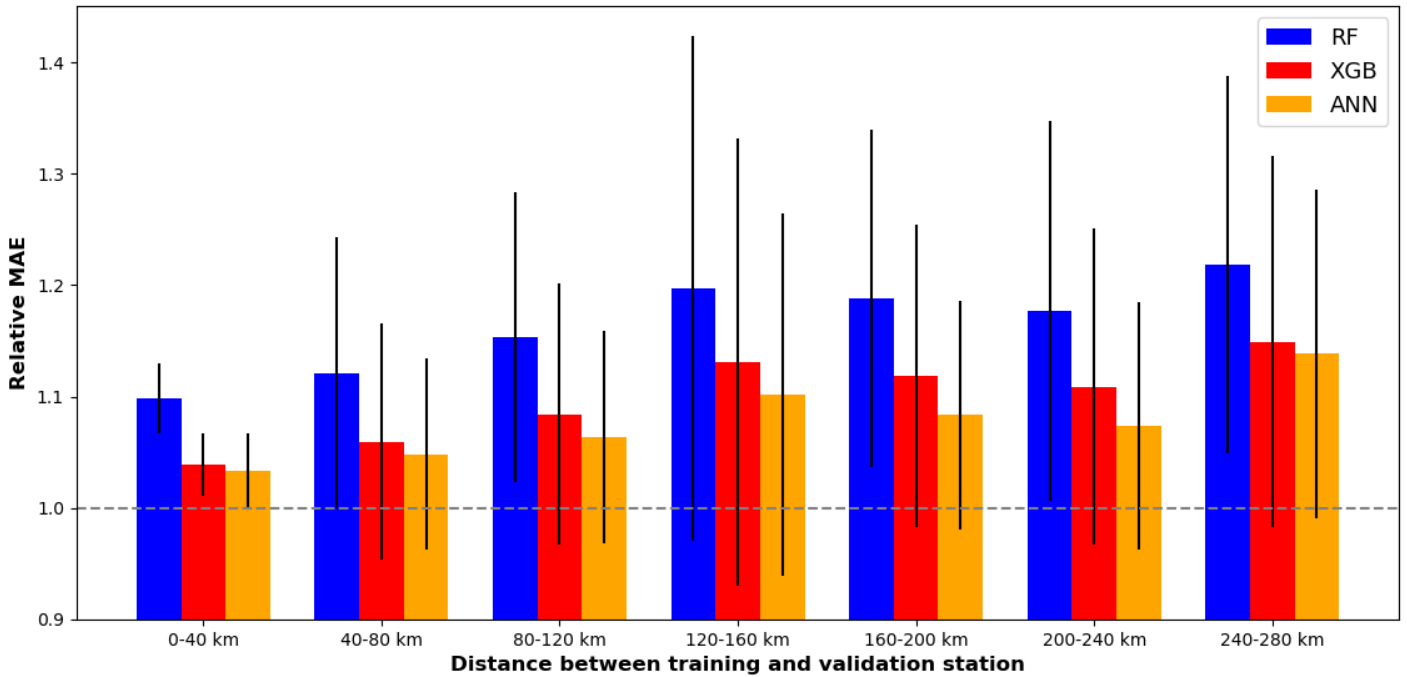
Figure 15: Relative MAE for different distance intervals.

5.4 Cardinal performance

To answer the fourth sub-question the cardinal direction between training and validation station is plotted against the relative error in a polar plot. The results are presented in figure 16. The error in each direction is calculated as the average validation error of stations in the particular direction. The black lines represent the standard deviation of the errors. From this figure it can be concluded that the relative error is significantly larger when the validation station is located west of the training station. Furthermore, the standard deviation is larger in this direction. The RF has an average relative error around 1.25 when validated to the west and 1.05 when validated to the east. This indicates that there is 20 % point difference in accuracy between validation to the west and east for RF. XGB shows similar results. However, relative errors are lower with a relative error of 1.20 to the west and 1.00 to the east. ANN shows fairly similar results compared to XGB, showing slightly lower relative errors to the west around 1.18.
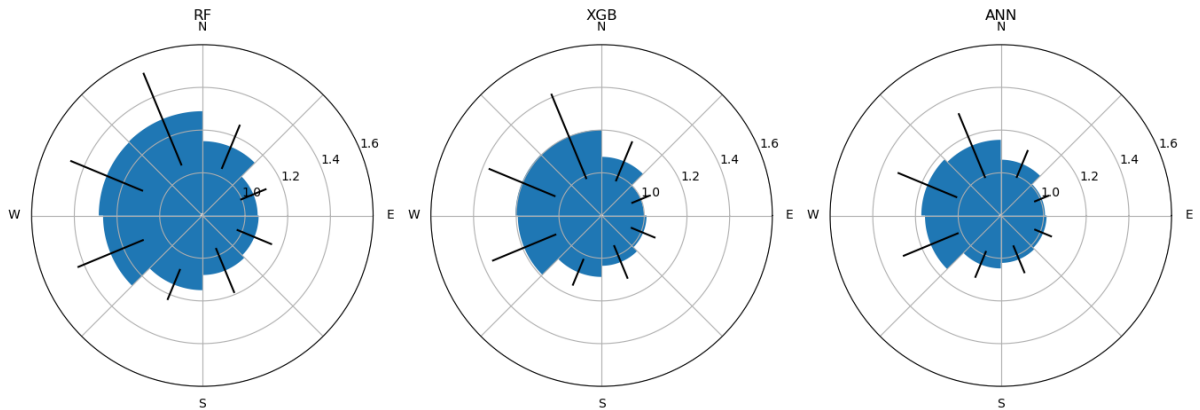
Figure 16: Cardinal performance of different MLMs based on relative MAE.

Results for the MAE and RMSE are comparable (appendix section A.4). The nRMSE figure shows different results. The nRMSE takes in to account the average solar irradiance of the validation station. Figure 17 shows the result of the MLMs based on the nRMSE. From this figure it can be denoted that the relative errors are more uniformly distributed. Relative errors are still larger to the west than to the east but differences are smaller. Therefore, different performances in a west and east validation direction are for some part a result of differences in average irradiance levels of the validation station.

To summarise, it can be concluded that there is a relation between the cardinal direction and the relative error. All MLMs show higher performances when validated in an eastern direction. For some part these results are caused by differences in irradiance levels between training and validation station. The ANN shows the lowest relative errors in all cardinal directions. Since most offshore stations are located north-west of onshore training stations higher relative errors can be expected. To estimate offshore irradiance and minimise relative errors it is recommended to use onshore stations that are located in the north-west part of the Netherlands.
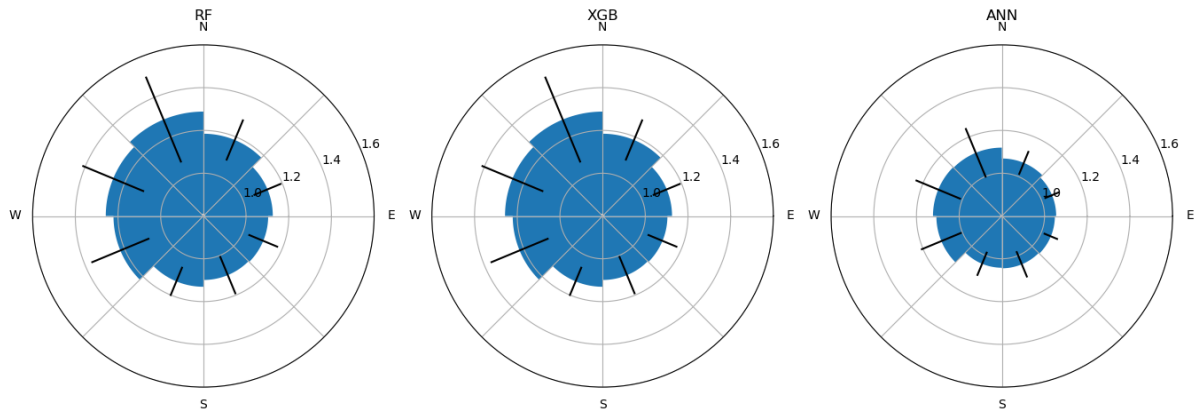
Figure 17: Cardinal performance of different MLMs based on relative nRMSE.

5.5 Temporal performance

To answer the fifth sub-question the MLMs are assessed on the temporal performance by keeping a fixed training interval with a varying validation interval and vice versa.

5.5.1 Fixed training interval
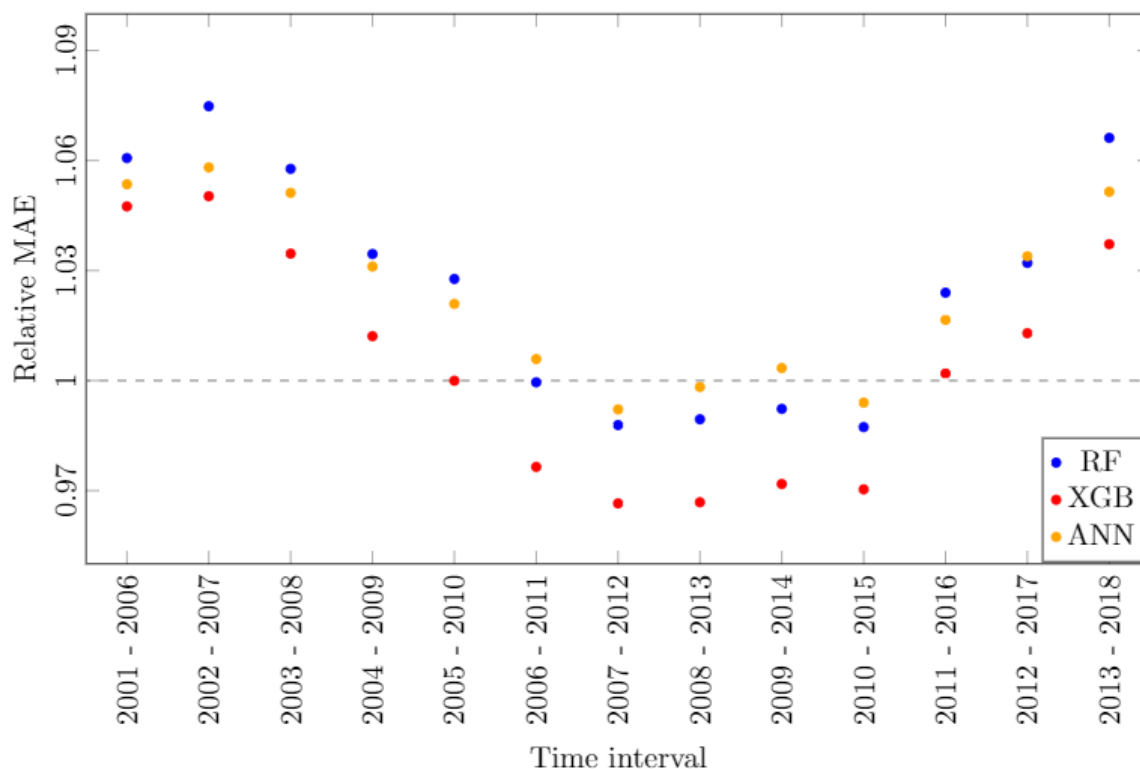
Figure 18: Relative MAE compared to a reference training interval in the period (2000-2005).

Figure 18 shows the relative MAE of a fixed training interval (2000-2005). Results for RMSE and nRMSE are similar to the results of MAE (appendix section A.4). The figure shows the relative errors for XGB are the lowest, while RF and ANN are slightly higher. Furthermore, it can be noted an increasing time difference between training and validation interval does not result in an increase of the relative error. Instead, the relative MAE is even declining until the interval (2007-2012). This indicates that an increasing temporal difference between training and validation data does not necessarily result in a lower performance of the MLMs.

5.5.2 Fixed validation interval
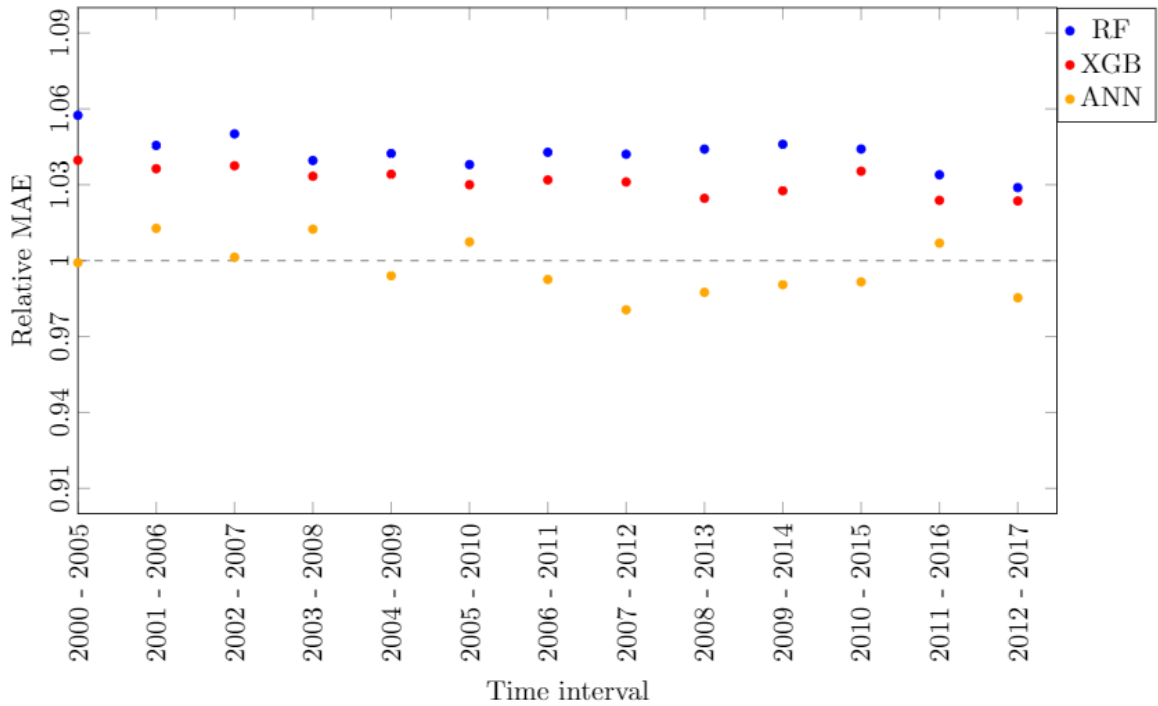
Figure 19: Relative MAE compared to a reference validation interval in the period (2013-2018).

Figure 19 shows the results for a fixed validation interval (2013-2018). Note that the same scale is used as in figure 18. The results are based on a varying training interval with a fixed validation interval. RMSE and nRMSE results are similar and can be found in appendix section A.4. Unlike the results of the fixed training interval, the results are fairly constant for varying training intervals. The ANN now shows the lowest relative errors as opposed to the results of the fixed training interval. This result shows that when the training interval changes, there is only a small change in relative error. Based on these results, selecting a specific training interval to estimate offshore irradiance is not desired.

To summarise, small differences in performance of the MLMs are found with a varying validation interval. There is no evidence that the performance of MLMs is affected if the time difference between training and validation interval increases. The results of the varying training interval prove that the performance of MLMs is barely affected by a changing training interval.

5.6 Offshore estimation

Based on the results found in sub-sections 5.1 until 5.5 offshore irradiance is estimated by selecting onshore stations based on certain criteria. First of all, the stations with comparable temperature, humidity and cloud cover are selected for the offshore estimation based on the feature importance found in section 5.1. Based on the results visualised in figures 20, 21 and 22, to estimate offshore irradiance, the stations De Kooy, Leeuwarden, Eelde and Vlissingen are selected. The bars indicate the annual mean and the black lines represent the standard deviations of the annual mean. De Kooy is selected because it has similar relative humidity, temperature and cloud cover levels compared to offshore values. Leeuwarden and Eelde have comparable temperature and humidity levels, and Vlissingen shows similar humidity and cloud cover levels.
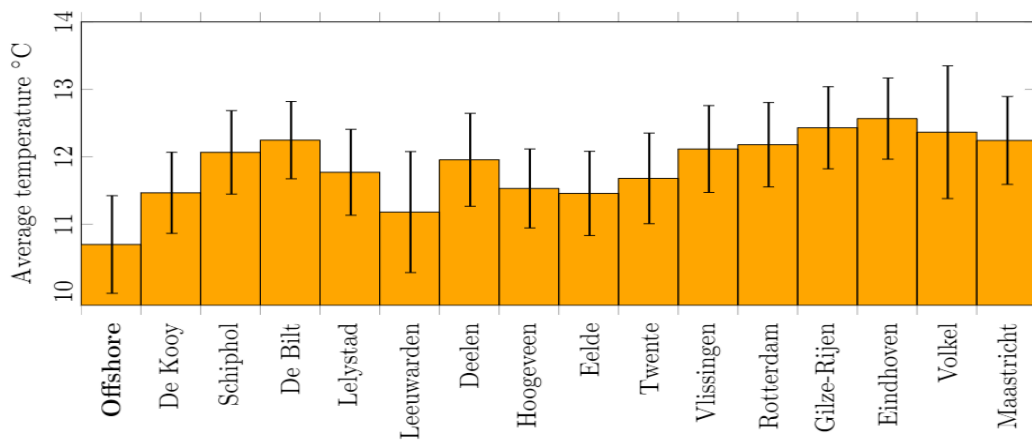
Figure 20: Average annual temperature (°C).
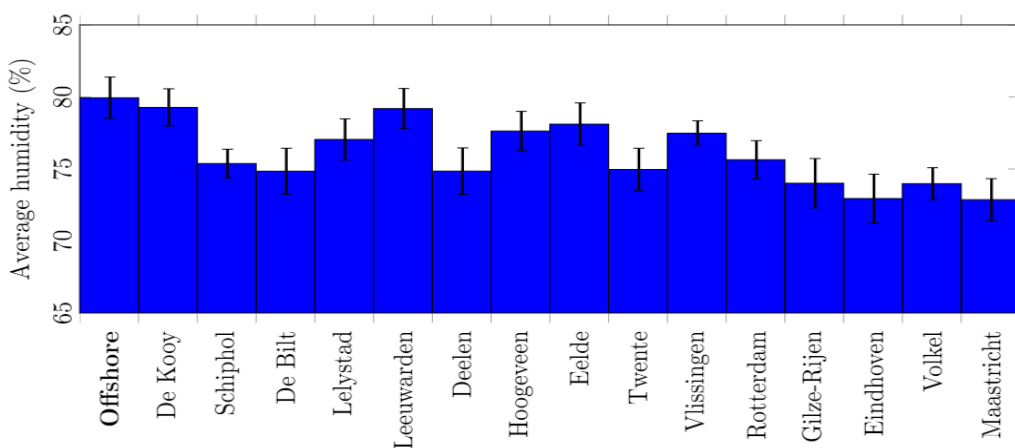
Figure 21: Average annual humidity (%).
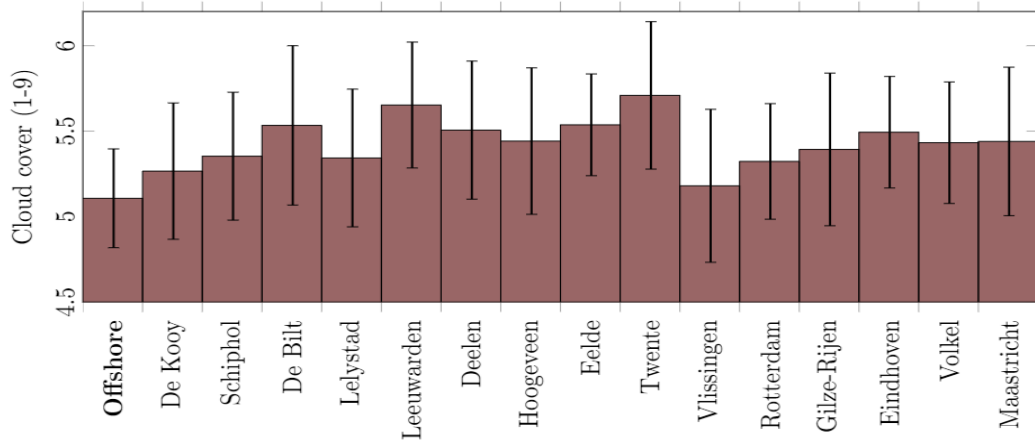
Figure 22: Average annual cloud cover (1-9).
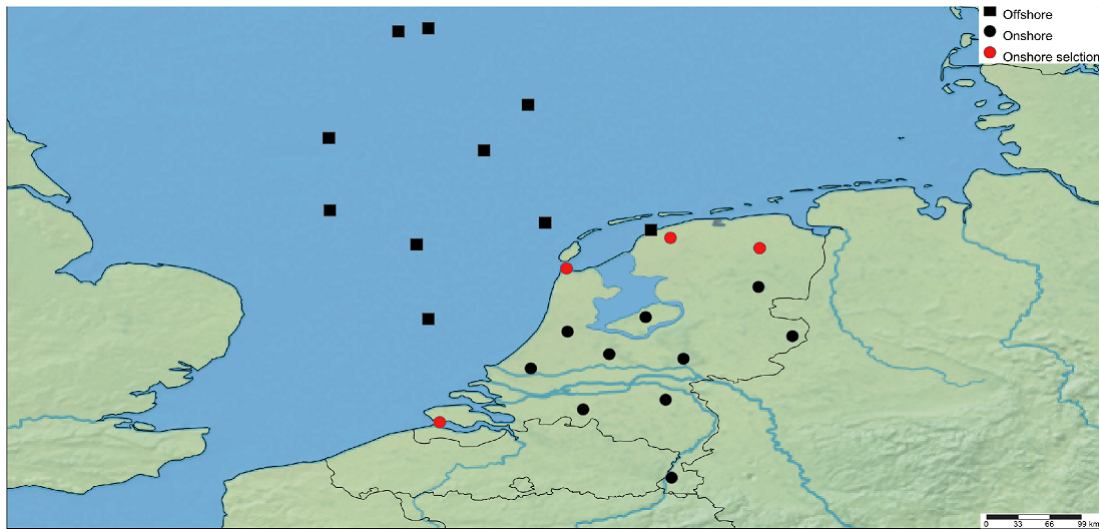
Figure 23: Onshore and offshore stations.

Figure 23 shows the stations selected to estimate offshore irradiance. This figure shows all of the onshore and offshore stations used in this research. The red dots represent the selected stations for the offshore estimation. These stations are all located near the coastline, which minimises the distance between training and validation stations. Training interval is selected in the period (2000-2018) and the validation interval is selected between (2012-2018). This validation interval is selected because in this period, average annual temperature differences between onshore and offshore stations are fairly constant as shown in figure 33 in the appendix section A.5. Finally, the ANN is used because this MLM has the lowest relative and absolute errors, hence minimising the bias-variance tradeoff.
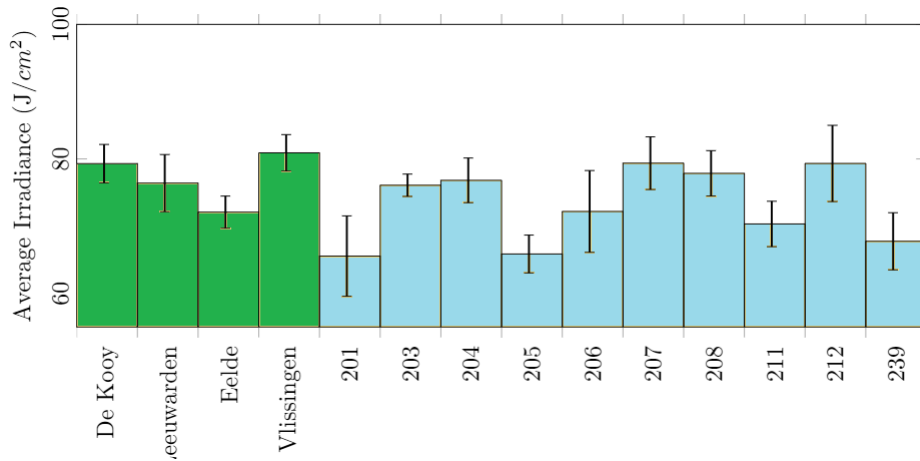
Figure 24: Irradiance levels for onshore (green) and offshore (blue) stations.

Figure 24 shows the results of the offshore estimation using the ANN. On average offshore irradiance levels are calculated to be 73.1 J/cm^2 compared to the onshore average of 75.6 J/cm^2. These results suggest that irradiance levels are slightly higher (3.5%) at onshore stations compared to offshore stations. In addition, for the various offshore stations there is a large difference between irradiance levels. Irradiance levels are comparatively low in stations 201, 205 and 239, while the irradiance levels in stations 212 and 207 are relatively high.

6   Discussion

From the offshore estimation it is concluded that onshore irradiance levels are 3.5% higher compared to offshore levels. The results of the onshore case study proved that the distance and cardinal direction between training and validation stations strongly affect the accuracy of the MLMs whereas temporal differences showed a smaller effect on the accuracy. To make conclusions on the performance of the MLMs estimating offshore irradiance, the results should be carefully interpreted and discussed.

6.1   Interpretation

- **Distance performance:** The results of this analysis showed a small increase of the relative error with increasing distances. It also showed that errors could increase be up to 50 percent in a range of small countries like the Netherlands. More important is that the standard deviation and thereby the uncertainty increases for larger distances. This is important to consider when estimating offshore irradiance where distances between onshore and offshore stations can be up to 500 km.

- **Cardinal performance:**
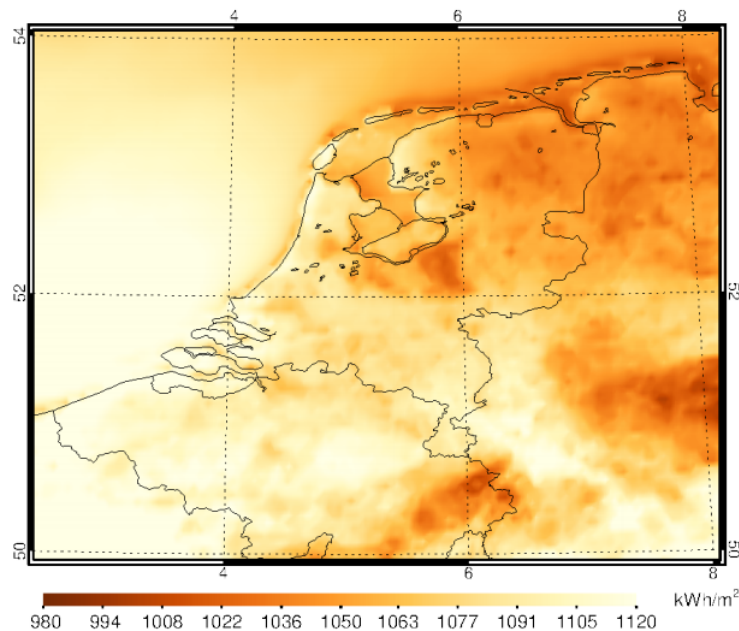
Figure 25: Irradiance levels based on satellite data in the period 2005-2017. Source: (Meirkink ,2018).

Figure 25 shows the average irradiance levels in the Netherlands and the North Sea in the period 2005-2017. These results are based on satellite data of Meteosat using infrared imaging.

This figure shows that offshore irradiance levels are higher compared to onshore levels. Based on this data the KNMI concluded the North Sea receives 4-8% more irradiance compared to onshore levels (Meirkink ,2018). This is a strong contradiction compared to the results of the offshore estimation in this study. In this study onshore irradiance was found to be 3.5 % higher. The results of the cardinal performance could be an explanation of this contradiction. Results of this analysis showed higher relative errors for models validated west of the training station. Models validated east of the training station showed significantly lower results. As mentioned in the results section, part of this is caused by differences in average irradiance levels between training and validation stations reflected by the nRMSE. Based on this result, there is a strong evidence that the validation accuracy is negatively affected when irradiance levels are higher at the validation station. Conversely, the accuracy is higher when models are validated for lower irradiance levels. Since most offshore stations are located north-west of the mainland, there is a strong reason to believe that the offshore estimation has considerable relative errors.

- **Temporal performance:** The results of the temporal performance assessment showed lower fluctuations of the relative error (0.97-1.07) compared to the distance and cardinal assessment. Especially the results of the fixed validation interval showed low variation in the relative error. The results of the fixed training interval showed minor variations in relative error. The question arises how this minor deviation can be explained. Figure 26 shows the same results as figure 18 but now the 5 year relative average temperature, irradiance and humidity compared to the reference interval are added to the plot. It is clearly visual from this figure that for all MLMs there is a strong Pearson correlation (Eq.13) between the temperature and the relative MAE. For relative humidity and irradiance, this relationship is lower. The correlation with other variables can be neglected. Table 8 presents the correlation between MAE and T, Q and U. It can be concluded that the temperature and the relative error are strongly correlated. Therefore, when selecting a validation interval, it is recommended to consider temperature differences between training and validation intervals.

MAE	T	Q	U
RF	0.695	0.126	0.205
XGB	0.619	0.221	0.322
ANN	0.624	0.099	-0.06

Table 8: Pearson correlation between relative MAE and the variables T, Q and U for the MLMs.
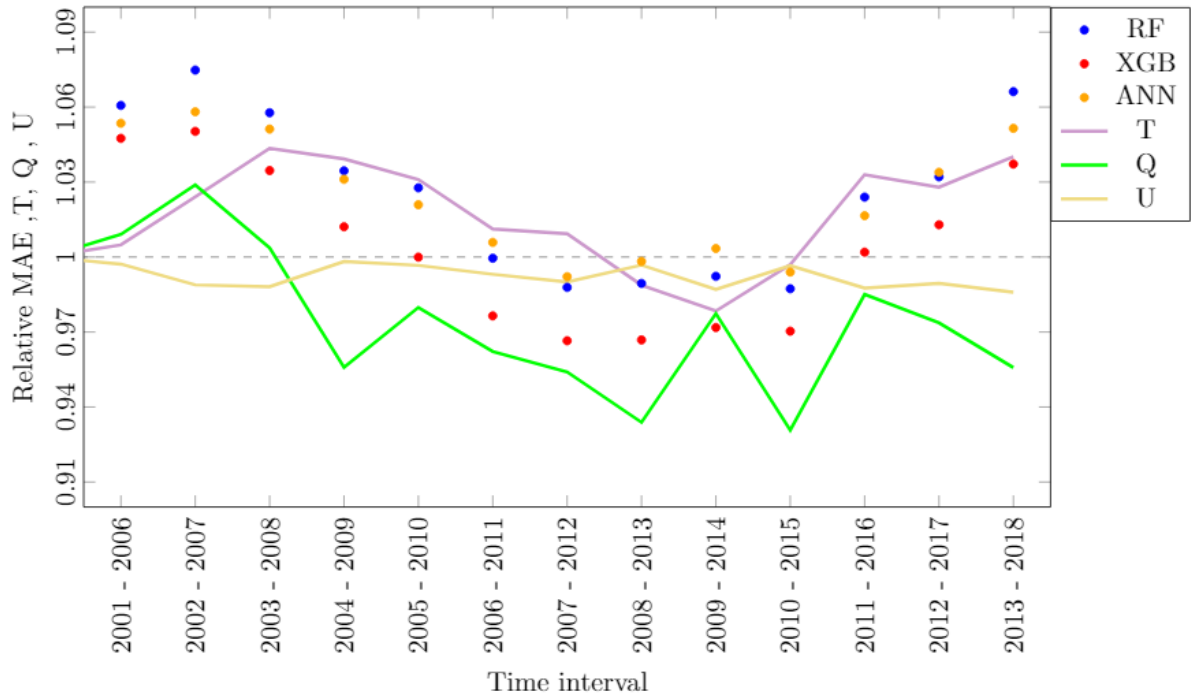
Figure 26: Relative MAE, T, Q and U compared to a reference training interval in the period (2000-2005).

Overall, this study should not be interpreted as an inarguable conclusion that when estimating solar irradiance, external factors always play a role. On the contrary, this research has shown that the accuracy of the MLM on a local scale is sometimes not affected by external factors or even improves (< 1) when estimating at other locations and time intervals. Therefore, when estimating solar irradiance, it is strongly suggested to take these effects into account before making conclusions about the performance of MLMs. Hence, this study should be interpreted as a guideline to determine to what extent results are influenced by these external factors.

6.2 Limitations

This research has several limitations to take into consideration. First of all the findings are based on a relatively small geographical scope. Results should be carefully interpreted if research is conducted on different geographical scales. Another limitations is the computational power. Due to this limitation the ANN design in the bias-variance section is solely based on training at station De Bilt, whereas RF and XGB are based on training at all stations. Nevertheless, it is expected that the design of the ANN would not change fundamentally if all stations were used. Finally, the conclusions on the performance of MLMs to estimate offshore irradiance are valuable for future solar resource estimation studies. There is however a strong need for offshore irradiance measurement

data in order to verify conclusions.

6.3 Further research

Similar evaluations should be carried out on both larger and smaller geographic scopes to see how external factors play a role on different scales. Next to this, installing irradiance measurement devices at offshore stations is strongly recommended in order to make accurate and concrete conclusions on the performance of MLMs. In addition, other estimation assessments should be performed to estimate offshore solar irradiance in order to accurately compare the performance of different estimation techniques. Including satellite data interpolation to estimate solar irradiance could be one such assessment. A research topic would be to compare the results of this assessment with a satellite data interpolation assessment to estimate solar irradiance at measurement stations. Since data on offshore irradiance is not yet available, an onshore case study similar to this study could be used to perform this assessment. Aguair et al.(2016) proposed to combine ground measurements with exogenous inputs provided by satellite and numerical weather prediction models data in order to improve intra-day solar forecasting. Therefore, the evaluation of MLMs using both ground- and satellite- based measurements as input to estimate solar irradiance in the North Sea is another potential research topic.

7 Conclusion

To answer the research question this research assessed the performance of the different MLMs to estimate the solar resource in the North Sea. In addition, it provided answers on the effects of the external factors, distance, cardinal direction and temporal differences on the performance of the MLMs. This research proves that MLMs are affected by external factors and therefore the results of the offshore estimations should be interpreted with caution. All MLMs have higher accuracy's compared to a linear regression model. The ANN shows the highest overall performance with an average MAE of approximately 21.5 J/cm^2 with a corresponding relative error of 1.10 percent, indicating that the estimation error increased by 10 percent on average when validation occurred elsewhere. XGB shows higher relative and absolute errors and RF has the lowest accuracy of the MLMs assessed. Based on the distance performance, it can be concluded that for all MLMs a small increase in relative error occurs when the distance increases. More importantly, the uncertainty increases with larger distances. Therefore, When estimating offshore irradiance large distances can potentially affect the performance of the MLMs. It also turned out that the cardinal direction

between training and validation station is important. Relative errors are substantially greater when model validation occurs west of the training station, whereas models validated east of the training station show almost no increase in relative error. The ANN has an average relative MAE around 1.18 when model validation occurs west of the training station and an average relative error around 1.0 when model validation occurs east of the training station. For all MLMs, temporal differences with a fixed training interval shows only small differences in relative errors between 0.96 and 1.06. For a significant part, these deviations are due to differences in temperature between training and validation intervals. Relative errors did not change significantly for a fixed validation interval. Estimates of offshore irradiance resulted in an average of 73.1 J/cm^2, which is lower than the onshore average of 75.6 J/cm^2. According to these results onshore irradiance levels are 3.5 % higher compared to offshore levels. These results are conflicting as a satellite based study by the KNMI concluded offshore irradiance levels are 4-8% higher compared to onshore levels. The final offshore estimations are therefore not unquestionable on the basis of this research since there is a relatively large distance between training and validation stations. Moreover, most offshore stations are located northwest of onshore stations. This direction showed high relative errors in the cardinal performance assessment. Based on the results of this study it can be concluded that the ANN has the best performance to estimate offshore irradiance. Based on the distance and cardinal direction between onshore and offshore stations the offshore estimation should be taken with consideration. To make strong conclusions on the performance of MLMs, accurate offshore irradiance measurements are desired.

References

[1] Aguiar, L. M., Pereira, B., Lauret, P., Díaz, F., David, M. (2016). *Combining solar irradiance measurements, satellite-derived data and a numerical weather prediction model to improve intra-day solar forecasting.* Renewable Energy, 97, 599-610.

[2] Breiman, L., (2001). *Random forests. Mach. Learn.* 45 (1), 5–32.

[3] Bhambhani, A. (2018, November 13). *Singapore's Sunseap Group Announces 5 MW Pilot Offshore Floating PV Project Along Straits Of Johor, North Of Woodlands Waterfront Park; Calls It World's First Largest Sea Water Floating PV System.* Taiyangnews. Retrieved March 11, 2019, from: http://taiyangnews.info/business/5-mw-offshore-floating-pv-project-in-se-asia/

[4] Chen, J. L., Liu, H. B., Wu, W., Xie, D. T. (2011). *Estimation of monthly solar radiation from measured temperatures using support vector machines–a case study.* Renewable Energy, 36(1), 413-420.

[5] Fan, J., Wang, X., Wu, L., Zhou, H., Zhang, F., Yu, X., Xiang, Y. (2018). *Comparison of Support Vector Machine and Extreme Gradient Boosting for predicting daily global solar radiation using temperature and precipitation in humid subtropical climates: A case study in China.* Energy conversion and management, 164, 102-111.

[6] Fortman, R.(2012). *Understanding the Bias-Variance Tradeoff.* http://scott.fortmann-roe.com/docs/BiasVariance.htmlfnref:4. 12 March, 2019.

[7] Friedman, J. H. (2001). *Greedy function approximation: a gradient boosting machine.* Annals of statistics, 1189-1232.

[8] Gala, Y., Fernández, Á., Díaz, J., Dorronsoro, J. R. (2016). *Hybrid machine learning forecasting of solar radiation values.* Neurocomputing, 176, 48-59.

[9] Goodfellow, I., Bengio, Y., Courville, A., (MIT). (2016). *Deep Learning.* Retrieved from: https://www.deeplearningbook.org/. Retrieved 12 December, 2018.

[10] Jang, H. S., Bae, K. Y., Park, H. S., Sung, D. K. (2016). *Solar power prediction based on satellite images and support vector machine.* IEEE Trans. Sustain. Energy, 7(3), 1255-1263.

[11] IEA World Energy Balances 2018. Retrieved from: https://webstore.iea.org/world-energy-balances-2018, 23 December 2018.

[12] Jain, A. K., Mao, J., Mohiuddin, K. M. (1996). *Artificial neural networks: A tutorial.* Computer, (3), 31-44.

[13] Johansson, B. (2013). *Security aspects of future renewable energy systems–A short overview.* Energy, 61, 598-605.

[14] Khare, Vikas, Nema, Baredar. *Solar–wind hybrid renewable energy system: A review.* Renewable and Sustainable Energy Reviews 58 (2016): 23-33.

[15] KNMI, 2018. Retrieved from: https://projects.knmi.nl/klimatologie/uurgegevens/selectie.cgi. 20 November,2018.

[16] Lauret, P., Voyant, C., Soubdhan, T., David, M., Poggi, P. (2015). *A benchmarking of machine learning methods for solar radiation forecasting in an insular context.* Solar Energy, 112, 446-457.

[17] Ma, L., Fu, T., Blaschke, T., Li, M., Tiede, D., Zhou, Z., Chen, D. (2017). *Evaluation of feature selection methods for object-based land cover mapping of unmanned aerial vehicle imagery using random forest and support vector machine classifiers.* ISPRS International Journal of Geo-Information, 6(2), 51.

[18] Marquez, R., Coimbra, C. F. (2011). *Forecasting of global and direct solar irradiance using stochastic learning methods, ground experiments and the NWS database.* Solar Energy, 85(5), 746-756.

[19] Mellit, A., Pavan, A. M. (2010). *A 24-h forecast of solar irradiance using artificial neural network: Application for performance prediction of a grid-connected PV plant at Trieste, Italy.* Solar Energy, 84(5), 807-821.

[20] Meirink,J.F., Koetse, W., Oudshoorn, C.(2018). *KNMI-activiteiten Zon Op Water.* KNMI. Retrieved from:https://www.zonopwater.nl/wp-content/uploads/2018/06/Meirink-14-juni-2018-Zon-op-Water.pdf. 18 April 2019.

[21] Miglietta, M. M., Huld, T., Monforti-Ferrario, F. (2017). *Local complementarity of wind and solar energy resources over Europe: an assessment study from a meteorological perspective.* Journal of Applied Meteorology and Climatology, 56(1), 217-234.

[22] Nikolakakis, T., Fthenakis, V. (2011). *The optimum mix of electricity from wind-and solar-sources in conventional power systems: Evaluating the case for New York State.* Energy Policy, 39(11), 6972-6980

[23] Oceans of Energy. (2018). *New consortium builds first offshore floating solar energy farm in the world Project 'Solar-at-Sea' starts.* Retrieved from: https://oceansofenergy.blue/press-release-1-new-consortium-builds-first-offshore/. December 13, 2018,

[24] Pinson, P., Christensen, L. E. A., Madsen, H., Sørensen, P. E., Donovan, M. H., Jensen, L. E. (2008). *Regime-switching modelling of the fluctuations of offshore wind generation.* Journal of Wind Engineering and Industrial Aerodynamics, 96(12), 2327-2347.

[25] Prasad, A. A., Taylor, R. A., Kay, M. (2017). *Assessment of solar and wind resource synergy in Australia.* Applied energy, 190, 354-367.

[26] PV-tech (2018), *Offshore floating solar. a technical perspective.*, (September, vol. 16 60–63.)

[27] Qi, Y. (2012). *Random forest for bioinformatics in Ensemble machine learning* (pp. 307-323). Springer, Boston, MA.

[28] Reddy, K. S., Ranjan, M. (2003). *Solar resource estimation using artificial neural networks and comparison with other correlation models.* Energy Conversion and Management, 44(15), 2519-2530.

[29] Rehman, S., Mohandes, M. (2008). *Artificial neural network estimation of global solar radiation using air temperature and relative humidity.* Energy Policy, 36(2), 571-576.

[30] Smits, G. F., Jordaan, E. M. (2002). *Improved SVM regression using mixtures of kernels.* In Neural Networks, 2002. IJCNN'02. Proceedings of the 2002 International Joint Conference on (Vol. 3, pp. 2785-2790). IEEE.

[31] Sözen, A., Arcaklioğlu, E., Özalp, M. (2004). *Estimation of solar potential in Turkey by artificial neural networks using meteorological and geographical data.* Energy Conversion and Management, 45(18-19), 3033-3052.

[32] Saeys, Y., Abeel, T., Van de Peer, Y. (2008, September). *Robust feature selection using ensemble feature selection techniques.* In Joint European Conference on Machine Learning and Knowledge Discovery in Databases (pp. 313-325). Springer, Berlin, Heidelberg.

[33] Sola, J., Sevilla, J. (1997). *Importance of input data normalization for the application of neural networks to complex industrial problems.* IEEE Transactions on nuclear science, 44(3), 1464-1468.

[34] United Nations(2017)., *Factsheet: People and Oceans.* Retrieved December 13, 2018, from https://www.un.org/sustainabledevelopment/wp-content/uploads/2017/05/Ocean-fact-sheet-package.pdf, 13 December 2018.

[35] Utrecht University (2018), *Universiteit Utrecht onderzoekt eerste drijvende zonnecentrale op zee.* Retrieved from: https://www.uu.nl/nieuws/universiteit-utrecht-onderzoekt-eerste-drijvende-zonnecentrale-op-zee-0. 20 January 2019.

[36] Voyant, C., Notton, G., Kalogirou, S., Nivet, M. L., Paoli, C., Motte, F., Fouilloy, A. (2017). *Machine learning methods for solar radiation forecasting: A review.* Renewable Energy, 105, 569-582.

[37] Voosen,P., (2018). *Vaclav Smil looks to history for the future of energy. What he sees is sobering.* Science 359 (6382), 1320-1324. DOI: 10.1126/science.359.6382.1320. Retrieved from: http://science.sciencemag.org/content/sci/359/6382/1320.full.pdf. 29 November,2018.

[38] Buijs, A., Nieuwenhuizen, W., Langers, F., Kramer, H. (2019). *Resultaten Nationale Landschapsenquête.* Wageningen University. Retrieved from: https://res.cloudinary.com/natuurmonumenten/raw/upload/v1552342578/2019-03/Resultaten-Nationale-Landschap-Enquete-Natuurmonumenten.pdf. April 11, 2019.

[39] Wind Europe. (2018). *World's First Offshore Wind Farm without Subsidies to be Built in the Netherlands.* Retrieved from: https://windeurope.org/newsroom/press-releases/worlds-first-offshore-wind-farm-without-subsidies-to-be-built-in-the-netherlands/. 25 November 2018.

[40] Zhang, Hengxu, (2018). *Quantitative synergy assessment of regional wind-solar energy resources based on MERRA reanalysis data.* Applied Energy 216 (2018): 172-182.

[41] Zheng, H., Yuan, J., Chen, L. (2017). *Short-term load forecasting using EMD-LSTM neural networks with a Xgboost algorithm for feature importance evaluation.* Energies, 10(8), 1168.

A   Appendix

A.1   Python scripts

A.1.1   RF script

```
1  from sklearn.ensemble import RandomForestRegressor
2
3  ## Random Forest
4  clist =[] # These parameters are used to check if there is one station (e.g.235) or
          two (235 and 240)
5  maemat=[] # matrix containt all MAE's between stations
6  rmsemat=[]  # matrix containt all RMSE's  between stations
7  nrmsemat=[] # matrix containt all nRMSE's  between stations
8  featimp = [] #used to calculate feature importances
9  for i in range(len(combi)): # For all combinations between stations
10
11     features= combi[i] # get one combination between stations
12     labels = features['Q'] # get irradiance dat
13     a = features['STN'] # These parameters are used to check if there is one station
          (e.g.235) or two (235 and 240)
14     b = np.mean(a) # These parameters are used to check if there is one station (e.g
          .235) or two (235 and 240)
15     c = features.iloc[0]['STN']# These parameters are used to check if there is one
          station (e.g.235) or two (235 and 240)
16     clist.append(c) # These parameters are used to check if there is one station (e.
          g.235) or two (235 and 240)
17     features= features.drop('STN', axis = 1) #Drop station from training variable
          list
18     features= features.drop('Q', axis = 1) # Drop irradiance from training variable
          list
19     feature_list = list(features.columns) #names of all the features
20
21     lf = len(features) # used to split training and validation data
22     ll = len(labels) # used to split training and validation data
23     if b == c: # If there is one station
24         train_features, test_features, train_labels, test_labels = train_test_split(
          features, labels, test_size = 0.25, random_state = 1)
25     if b != c: # If there are two stations
26         lfh = int(lf*0.5) #make sure that test data is from the first station and
          validation data from the second station
27         llh = int(ll*0.5) #make sure that test data is from the first station and
```

```
      validation data from the second station
28        train_features ,no, train_labels ,nope= train_test_split(features [0:lfh],
      labels [0:llh], test_size = 0.25, random_state = 1)
29        no, test_features, nope, test_labels = train_test_split(features [lfh:lf],
      labels [llh:ll], test_size = 0.25, random_state = 1)
30        del no, nope #ignore
31
32 #perform random forest
33    trees =50 # number of trees
34    k=10 # number of layers
35    if i==0 or clist [i−1]!= c: #for first training station or new training station
36        rf = RandomForestRegressor(n_estimators=trees, random_state = 1, max_depth =
      k, max_features=10)
37        rf.fit(train_features, train_labels);
38
39        ##Get numerical feature importances (Shows which variables are most
      important)
40        importances = list(rf.feature_importances_)
41        featimp.append(importances)
42        la=featimp
43        ncols = len(la [0])
44        nrows = len(la)
45        # Sum all elements in each column:
46        results = ncols *[0] # sums per column, afterwards average
47        for col in range(ncols):
48            for row in range(nrows):
49                results [col] += la [row][col]
50                # Then calculate averages:
51                # nrows is also number of elements in every col:
52        nelem = float(nrows)
53        importances = [s/nelem for s in results]
54         #List of tuples with variable and importance
55        feature_importances = [(feature, round(importance, 4)) for feature,
      importance in zip(feature_list, importances)]
56          #Sort the feature importances by most important first
57        feature_importances = sorted(feature_importances, key = lambda x: x[1],
      reverse = True)
58
59    #Use the forest's predict method on the test data
60    predictions = rf.predict(test_features)
61    # Calculate the absolute errors
```

52

```python
62     errors = abs(predictions − test_labels)

63

64     mae = (np.mean(errors))
65     maemat.append(mae) # create list containing all erros between stations

66

67     rmse = sqrt(np.mean((errors*errors)))
68     rmsemat.append(rmse) # create list containing all erros between stations

69

70     nrmse= rmse/(np.mean(test_labels))
71     nrmsemat.append(nrmse) # create list containing all erros between stations

72

73

74

75     print((len(maemat)/225)*100,'%' ) # show progress

76

77 # This part marices are created that contain all absolute and relative errors
       between stations

78

79 maematrix = pd.DataFrame(index=Distance.index, columns=Distance.index) #Create
       Error matrix
80 savemae = pd.DataFrame(index=Distance.index, columns=Distance.index)

81

82 rmsematrix = pd.DataFrame(index=Distance.index, columns=Distance.index) #Create
       Error matrix
83 savermse = pd.DataFrame(index=Distance.index, columns=Distance.index)

84

85 nrmsematrix = pd.DataFrame(index=Distance.index, columns=Distance.index) #Create
       Error matrix
86 savenrmse = pd.DataFrame(index=Distance.index, columns=Distance.index)

87

88 def ermat(x,y,u):
89     k=−1
90     for i in range(len(x)):
91         for j in range(len(x)):
92             k=k+1
93             x.iloc[[i], [j]]= y[k]  #store all errors in matrix
94             u.iloc[[i], [j]]= y[k]
95     Diagonal =[] # matrix is divided by diagonal to calculate relative performance
96     for i in range (0,15):
97         D = x.iloc[i,i]
98         Diagonal.append(D)
```

53

```
99        for  i  in  range(len(x)):
100            x.iloc[i] = x.iloc[i]/Diagonal[i]
101        return x,u
102
103
104 ermat(maematrix,maemat,savemae) # maematrix = relative  error  &  savemae  =  relative
           error
105 ermat(rmsematrix,rmsemat,savermse)
106 ermat(nrmsematrix,nrmsemat,savenrmse)
```

A.1.2 XGB script

XGB script is similar to RF script. Only the following lines are adjusted:

```
1 #Random  forest  script:
2 #from  sklearn.ensemble  import  RandomForestRegressor
3 #trees =50 # number  of  trees
4    #k=10 # number  of  layers
5        # rf = RandomForestRegressor(n_estimators=trees, #random_state = 1,
6        #max_depth =k,  max_features=10)
7        #rf.fit(train_features,  train_labels);
8        #predictions = rf.predict(test_features)
9
10
11 # Extreme  Gradient  Boosting  script
12 from  sklearn.ensemble  import  GradientBoostingRegressor
13 trees = 100
14    k=4
15    l= 0.1
16    gb = GradientBoostingRegressor(n_estimators=trees,  learning_rate = l,
        random_state = 1,  max_depth =k,loss='ls',  criterion ='mse')
17    gb.fit(train_features,  train_labels);
18    predictions = gb.predict(test_features)
```

A.1.3 ANN script

```
1 ## Artificial  Neural  Network
2 import  tensorflow  as  tf
3 from  tensorflow  import  keras
4 from  tensorflow.keras  import  layers
5 clist =[]
6 maemat=[]
7 rmsemat=[]
```

```
 8  nrmsemat=[]

 9

10  for  i  in  range(len(combi)): # For  all  combinations  between  stations

11

12      features= combi[i] # get  one  combination  from  combi  list
13      #labels = features['Q'] # define  the  target  of  the  ANN
14      a = features['STN'] # These  parameters  are  used  to  check  if  there  is  one  station
                (e.g.235)  or  two  (235  and  240)
15      b = np.mean(a) # These  parameters  are  used  to  check  if  there  is  one  station  (e.g
               .235)  or  two  (235  and  240)
16      c = features.iloc[0]['STN'] # These  parameters  are  used  to  check  if  there  is  one
                station  (e.g.235)  or  two  (235  and  240)
17      clist.append(c)
18      features= features.drop('STN',  axis = 1) #Drop  station  from  training  variable
                list
19      labels= features['Q']
20      features= features.drop('Q',  axis = 1) # Drop  irradiance  from  training  variable
                list
21      feature_list = list(features.columns) #names  of  all  the  features

22

23      lf = len(features) # used  to  split  training  and  validation  data
24      ll = len(labels) # used  to  split  training  and  validation  data
25      if  b == c: # If  there  is  one  station

26

27         X_train, X_test, Y_train, Y_test = sk.train_test_split(features,labels,
         test_size=0.25,  random_state = 1)
28      if  b != c: # If  there  are  two  stations
29          lfh = int(lf*0.5)
30          llh = int(ll*0.5)
31          X_train,no,Y_train,nope= sk.train_test_split(features[0:lfh],  labels[0:llh],
          test_size = 0.25,  random_state = 1) #make  sure  that  test  data  is  from  the
        first  station  and  validation  data  from  the  second  station
32          no, X_test, nope, Y_test = sk.train_test_split(features[lfh:lf],  labels[llh:
         ll],  test_size = 0.25,  random_state = 1) #make  sure  that  test  data  is  from  the
        first  station  and  validation  data  from  the  second  station

33

34          del  no,  nope  #ignore
35      # Data  normalisation
36      Xtr_n = X_train['N']/9
37      X_train.update(Xtr_n)
```

```python
38    Xtr_nor= (X_train[['DD','FH','FF','FX', 'T', 'TD', 'P', 'VV', 'U']]-X_train[['DD
      ','FH','FF','FX', 'T', 'TD', 'P', 'VV', 'U']].mean())/X_train[['DD','FH','FF','
      FX', 'T', 'TD', 'P', 'VV', 'U']].std()
39    X_train.update(Xtr_nor)
40  # Data normalisation
41    Xt_n = X_test['N']/9
42    X_test.update(Xt_n)
43    Xt_nor= (X_test[['DD','FH','FF','FX', 'T', 'TD', 'P', 'VV', 'U']]-X_test[['DD','
      FH','FF','FX', 'T', 'TD', 'P', 'VV', 'U']].mean())/X_test[['DD','FH','FF','FX',
       'T', 'TD', 'P', 'VV', 'U']].std()
44    X_test.update(Xt_nor)
45
46    if i==0 or clist[i-1]!= c: #for first training station or new training station
47        def build_model():
48            model = keras.Sequential([
49            layers.Dense(16, activation=tf.nn.sigmoid, input_shape=[X_train.shape
      [1]]),
50            layers.Dense(16, activation=tf.nn.sigmoid),
51            layers.Dense(16, activation=tf.nn.sigmoid),  layers.Dense(1)])
52
53
54            optimizer = tf.keras.optimizers.RMSprop(0.005)
55
56            model.compile(loss='mse',
57                optimizer=optimizer,
58                metrics=['mae', 'mse'])
59            return model
60
61        model = build_model()
62        model.summary()
63
64
65        # Display training progress by printing a single dot for each completed
      epoch
66        class PrintDot(keras.callbacks.Callback):
67            def on_epoch_end(self, epoch, logs):
68                if epoch % 100 == 0: print('')
69                print('.', end='')
70
71        EPOCHS = 100
72        BATCH= 20
```

```python
73
74          history = model.fit( X_train, Y_train, epochs=EPOCHS, batch_size=BATCH,
       validation_split = 0.25, verbose=0,callbacks=[PrintDot()])
75
76          hist = pd.DataFrame(history.history)
77          hist['epoch'] = history.epoch
78          hist.tail()
79
80
81          loss, mae, mse = model.evaluate(X_test, Y_test, verbose=0)
82          maemat.append(mae)
83          rmse = sqrt(mse)
84          rmsemat.append(rmse)
85          nrmse =rmse/(np.mean(Y_test))
86          nrmsemat.append(nrmse)
87          print("Testing set Mean Abs Error: {:5.2f} MPG".format(mae))
88
89
90      else:
91          loss, mae, mse = model.evaluate(X_test, Y_test, verbose=0)
92          maemat.append(mae)
93          rmse = sqrt(mse)
94          rmsemat.append(rmse)
95          nrmse =rmse/(np.mean(Y_test))
96          nrmsemat.append(nrmse)
97          print("Testing set Mean Abs Error: {:5.2f} MPG".format(mae))
98
99      print((i/225)*100,'%' ) # show progress
100
101 maematrix = pd.DataFrame(index=Distance.index, columns=Distance.index) #Create
       Error matrix
102 savemae = pd.DataFrame(index=Distance.index, columns=Distance.index)
103
104 rmsematrix = pd.DataFrame(index=Distance.index, columns=Distance.index) #Create
       Error matrix
105 savermse = pd.DataFrame(index=Distance.index, columns=Distance.index)
106
107 nrmsematrix = pd.DataFrame(index=Distance.index, columns=Distance.index) #Create
       Error matrix
108 savenrmse = pd.DataFrame(index=Distance.index, columns=Distance.index)
109
```

```python
110  def ermat(x,y,u):
111      k=-1
112      for i in range(len(x)):
113          for j in range(len(x)):
114              k=k+1
115              x.iloc[[i], [j]]= y[k]   #store all errors in matrix
116              u.iloc[[i], [j]]= y[k]
117      Diagonal =[] # matrix is divided by diagonal to calculate relative performance
118      for i in range (0,15):
119          D = x.iloc[i,i]
120          Diagonal.append(D)
121      for i in range(len(x)):
122          x.iloc[i] = x.iloc[i]/Diagonal[i]
123      return x,u
124
125
126
127  ermat(maematrix,maemat,savemae) #maematrix = relative error & savmae = absolute
         error
128  ermat(rmsematrix,rmsemat,savermse)
129  ermat(nrmsematrix,nrmsemat,savenrmse)
```

A.2 Hyperparameter optimisation

Max Features F	Absolute			Relative		
	MAE	*RMSE*	*nRMSE*	*MAE*	*RMSE*	*nRMSE*
F=3	25.03	34.94	0.46	1.120	1.130	1.129
F=5	23.31	33.69	0.44	1.138	1.148	1.147
F=10	22.67	33.41	0.44	1.149	1.159	1.158
F=15(All)	22.67	33.49	0.44	1.154	1.164	1.163

Table 9: Absolute and relative errors for different number of max features (F) in RF.

K layers	Absolute			Relative		
	MAE	*RMSE*	*nRMSE*	*MAE*	*RMSE*	*nRMSE*
K=3	23.68	33.75	0.445	1.076	1.085	1.085
K=4	22.93	33.12	0.437	1.092	1.099	1.099
K=5	22.48	32.75	0.432	1.114	1.120	1.120

Table 10: Absolute and relative errors for different number of layers (K) in XGB.

Optimizer	Absolute			Relative		
	MAE	*RMSE*	*nRMSE*	*MAE*	*RMSE*	*nRMSE*
RMSprop	21.62	31.54	0.415	1.086	1.083	1.043
SGD	21.66	32.10	0.423	1.105	1.110	1.055
Adagrad	65.99	97.05	1.280	1.036	1.035	0.998
Adadelta	68.91	102.3	1.349	1.037	1.034	0.997
Adam	21.91	31.94	0.421	1.091	1.088	1.048
Adamax	22.73	32.29	0.425	1.077	1.079	1.039
Nadam	21.67	31.69	0.417	1.088	1.085	1.045

Table 11: Absolute and relative errors for different optimisers.

Learning rate	Absolute			Relative		
	MAE	*RMSE*	*nRMSE*	*MAE*	*RMSE*	*nRMSE*
0.001	21.66	31.74	0.418	1.093	1.089	1.049
0.005	21.64	31.68	0.417	1.089	1.082	1.042
0.01	21.64	31.89	0.420	1.103	1.096	1.055
0.05	23.89	34.60	0.456	1.070	1.069	1.029

Table 12: Absolute and relative errors for different learning rates.

Activation Function	Absolute			Relative		
	MAE	*RMSE*	*nRMSE*	*MAE*	*RMSE*	*nRMSE*
Sigmoid	21.64	31.68	0.417	1.089	1.082	1.042
Softmax	22.23	32.43	0.427	1.098	1.090	1.050
Softplus	21.74	32.08	0.423	1.101	1.097	1.056
Softsign	22.14	32.02	0.422	1.090	1.084	1.044
Relu	21.63	31.47	0.415	1.099	1.095	1.055
Tanh	22.01	32.55	0.429	1.100	1.095	1.055
Hard sigmoid	21.87	31.76	0.418	1.094	1.089	1.048
Linear	33.31	42.97	0.567	1.044	1.050	1.012

Table 13: Absolute and relative errors for different activation functions.

A.3 Absolute and relative errors between stations

	235	240	260	269	270	275	279	280	290	310	344	350	370	375	380
235	1.0	0.89	0.89	0.88	0.84	0.89	0.84	0.84	0.89	0.97	0.92	0.91	0.92	0.91	0.94
240	1.53	1.0	1.06	1.08	1.17	1.08	1.04	1.05	1.11	1.34	1.1	1.09	1.12	1.11	1.15
260	1.71	1.16	1.0	1.17	1.32	1.1	1.1	1.13	1.13	1.51	1.19	1.11	1.13	1.13	1.18
269	1.54	1.12	1.1	1.0	1.18	1.11	1.05	1.06	1.14	1.38	1.14	1.14	1.17	1.14	1.18
270	1.4	1.15	1.15	1.1	1.0	1.15	1.07	1.06	1.17	1.33	1.17	1.2	1.22	1.2	1.23
275	1.71	1.2	1.11	1.18	1.33	1.0	1.11	1.15	1.12	1.52	1.23	1.11	1.12	1.13	1.18
279	1.63	1.18	1.13	1.13	1.24	1.12	1.0	1.09	1.16	1.45	1.21	1.16	1.19	1.16	1.21
280	1.57	1.18	1.14	1.13	1.19	1.13	1.07	1.0	1.16	1.43	1.21	1.17	1.2	1.18	1.23
290	1.65	1.18	1.09	1.15	1.29	1.06	1.07	1.11	1.0	1.48	1.21	1.09	1.09	1.1	1.15
310	1.3	1.05	1.07	1.04	1.05	1.07	1.01	1.01	1.07	1.0	1.08	1.11	1.12	1.11	1.11
344	1.53	1.08	1.07	1.07	1.16	1.09	1.04	1.05	1.1	1.35	1.0	1.11	1.14	1.13	1.16
350	1.71	1.19	1.08	1.18	1.34	1.07	1.09	1.13	1.1	1.54	1.22	1.0	1.1	1.11	1.17
370	1.72	1.22	1.1	1.2	1.37	1.07	1.11	1.15	1.09	1.55	1.24	1.1	1.0	1.11	1.16
375	1.63	1.16	1.07	1.14	1.28	1.04	1.06	1.1	1.06	1.48	1.19	1.09	1.07	1.0	1.12
380	1.57	1.13	1.06	1.1	1.24	1.03	1.04	1.07	1.05	1.41	1.15	1.08	1.07	1.07	1.0

Table 14: Relative MAE RF.

	235	240	260	269	270	275	279	280	290	310	344	350	370	375	380
235	26.83	23.9	23.94	23.49	22.56	23.8	22.5	22.44	23.88	25.93	24.59	24.48	24.77	24.52	25.28
240	29.84	19.52	20.64	21.01	22.8	21.17	20.38	20.48	21.66	26.2	21.52	21.36	21.93	21.64	22.5
260	31.65	21.43	18.51	21.66	24.42	20.37	20.36	20.88	20.83	27.99	22.06	20.46	20.83	20.92	21.93
269	29.67	21.68	21.28	19.28	22.71	21.38	20.25	20.4	21.98	26.59	22.05	21.95	22.48	22.04	22.73
270	27.89	22.95	22.81	21.96	19.89	22.96	21.32	20.99	23.37	26.44	23.27	23.84	24.35	23.82	24.55
275	31.84	22.44	20.66	21.94	24.81	18.66	20.72	21.38	20.95	28.43	23.01	20.63	20.87	21.08	21.94
279	30.36	22.03	21.12	21.17	23.09	20.83	18.67	20.43	21.74	27.16	22.56	21.71	22.18	21.75	22.53
280	29.45	22.12	21.36	21.15	22.39	21.22	20.0	18.77	21.86	26.92	22.64	21.91	22.53	22.16	23.07
290	31.2	22.29	20.51	21.81	24.4	20.02	20.21	20.92	18.9	28.04	22.87	20.61	20.69	20.75	21.75
310	28.22	22.9	23.21	22.61	22.88	23.17	21.97	21.91	23.37	21.75	23.45	24.12	24.36	24.14	24.25
344	29.86	20.97	20.75	20.76	22.57	21.13	20.26	20.38	21.46	26.27	19.47	21.64	22.2	21.92	22.6
350	31.92	22.12	20.18	21.92	24.94	19.99	20.34	21.14	20.45	28.75	22.7	18.65	20.46	20.75	21.74
370	32.11	22.75	20.53	22.38	25.66	19.96	20.74	21.57	20.41	29.06	23.12	20.63	18.72	20.69	21.71
375	31.26	22.23	20.44	21.91	24.62	20.04	20.3	21.07	20.38	28.44	22.77	20.84	20.57	19.18	21.54
380	31.11	22.42	21.05	21.81	24.66	20.43	20.59	21.16	20.83	27.92	22.72	21.3	21.26	21.25	19.81

Table 15: Absolute MAE RF.

	235	240	260	269	270	275	279	280	290	310	344	350	370	375	380
235	1.0	0.9	0.91	0.89	0.85	0.9	0.86	0.86	0.9	0.96	0.92	0.92	0.93	0.92	0.96
240	1.57	1.0	1.06	1.09	1.19	1.09	1.06	1.07	1.12	1.39	1.1	1.1	1.13	1.1	1.17
260	1.77	1.17	1.0	1.19	1.35	1.1	1.12	1.16	1.13	1.58	1.2	1.1	1.12	1.12	1.2
269	1.57	1.11	1.1	1.0	1.19	1.11	1.06	1.07	1.13	1.42	1.13	1.13	1.15	1.13	1.18
270	1.41	1.15	1.15	1.12	1.0	1.17	1.09	1.08	1.18	1.34	1.16	1.2	1.22	1.19	1.24
275	1.76	1.21	1.11	1.2	1.36	1.0	1.13	1.17	1.13	1.58	1.24	1.1	1.11	1.12	1.19
279	1.64	1.16	1.11	1.13	1.23	1.11	1.0	1.1	1.15	1.47	1.18	1.14	1.16	1.13	1.2
280	1.58	1.15	1.12	1.12	1.19	1.12	1.07	1.0	1.15	1.45	1.18	1.14	1.17	1.15	1.21
290	1.69	1.18	1.08	1.17	1.31	1.06	1.09	1.12	1.0	1.52	1.2	1.08	1.08	1.08	1.16
310	1.32	1.07	1.09	1.08	1.06	1.1	1.04	1.05	1.1	1.0	1.09	1.13	1.14	1.12	1.15
344	1.58	1.08	1.07	1.09	1.18	1.1	1.06	1.07	1.11	1.38	1.0	1.12	1.14	1.12	1.17
350	1.78	1.2	1.09	1.2	1.37	1.08	1.12	1.16	1.1	1.6	1.24	1.0	1.09	1.11	1.18
370	1.78	1.23	1.11	1.23	1.41	1.08	1.14	1.18	1.11	1.61	1.26	1.11	1.0	1.1	1.18
375	1.69	1.18	1.08	1.18	1.32	1.06	1.09	1.13	1.08	1.54	1.21	1.1	1.08	1.0	1.15
380	1.59	1.11	1.04	1.1	1.24	1.02	1.04	1.07	1.03	1.43	1.13	1.05	1.05	1.05	1.0

Table 16: Relative RMSE RF.

	235	240	260	269	270	275	279	280	290	310	344	350	370	375	380
235	38.09	34.13	34.49	33.83	32.43	34.36	32.83	32.82	34.4	36.61	35.02	35.2	35.4	34.91	36.42
240	44.99	28.6	30.45	31.23	33.96	31.29	30.45	30.71	31.99	39.63	31.6	31.43	32.24	31.6	33.45
260	48.69	32.08	27.47	32.73	37.11	30.3	30.76	31.8	30.98	43.33	33.02	30.28	30.82	30.75	32.85
269	44.34	31.47	31.07	28.25	33.53	31.33	30.07	30.29	32.07	39.98	31.93	31.84	32.54	31.92	33.36
270	40.6	32.99	33.12	32.12	28.8	33.6	31.43	31.04	34.03	38.53	33.42	34.57	35.26	34.27	35.73
275	48.18	33.23	30.4	32.91	37.29	27.41	31.0	32.17	30.91	43.34	33.91	30.08	30.35	30.66	32.55
279	45.24	31.96	30.75	31.23	34.01	30.59	27.62	30.31	31.74	40.59	32.7	31.46	32.04	31.32	33.05
280	43.67	31.79	30.85	30.95	32.82	31.08	29.52	27.66	31.76	40.11	32.54	31.61	32.4	31.77	33.48
290	47.18	32.97	30.15	32.65	36.59	29.61	30.46	31.36	27.98	42.53	33.71	30.24	30.34	30.29	32.42
310	41.11	33.37	33.86	33.52	33.08	34.21	32.48	32.59	34.15	31.18	34.06	35.31	35.49	34.85	35.85
344	44.94	30.8	30.6	30.95	33.71	31.4	30.34	30.48	31.62	39.45	28.52	31.84	32.61	32.02	33.39
350	48.74	32.95	29.9	33.03	37.6	29.54	30.78	31.8	30.33	43.96	33.94	27.45	29.98	30.36	32.48
370	49.16	34.05	30.5	33.87	38.85	29.75	31.48	32.57	30.52	44.45	34.75	30.57	27.58	30.4	32.65
375	47.44	33.09	30.13	32.99	37.03	29.69	30.66	31.63	30.25	43.26	33.85	30.69	30.2	28.02	32.23
380	46.96	32.85	30.75	32.54	36.68	30.12	30.72	31.48	30.45	42.04	33.44	31.04	30.97	30.83	29.47

Table 17: Absolute RMSE RF.

	235	240	260	269	270	275	279	280	290	310	344	350	370	375	380
235	1.0	0.95	0.99	0.96	0.89	0.98	0.94	0.95	0.97	0.95	0.97	0.98	0.99	0.92	1.02
240	1.51	1.0	1.11	1.12	1.17	1.13	1.1	1.12	1.14	1.3	1.11	1.11	1.14	1.05	1.19
260	1.63	1.13	1.0	1.17	1.28	1.09	1.11	1.16	1.1	1.42	1.16	1.07	1.09	1.02	1.16
269	1.47	1.1	1.12	1.0	1.15	1.12	1.07	1.09	1.13	1.3	1.11	1.11	1.14	1.05	1.17
270	1.37	1.17	1.22	1.16	1.0	1.22	1.14	1.14	1.22	1.27	1.18	1.22	1.26	1.15	1.27
275	1.63	1.19	1.13	1.19	1.3	1.0	1.13	1.19	1.12	1.44	1.2	1.07	1.09	1.03	1.17
279	1.52	1.13	1.13	1.12	1.17	1.11	1.0	1.11	1.13	1.34	1.15	1.11	1.14	1.05	1.18
280	1.45	1.11	1.12	1.1	1.12	1.12	1.08	1.0	1.12	1.31	1.13	1.1	1.14	1.05	1.18
290	1.58	1.17	1.1	1.17	1.26	1.07	1.13	1.14	1.0	1.4	1.19	1.07	1.08	1.01	1.15
310	1.35	1.15	1.21	1.17	1.11	1.21	1.17	1.16	1.2	1.0	1.17	1.21	1.23	1.13	1.24
344	1.51	1.09	1.12	1.11	1.16	1.14	1.12	1.11	1.14	1.29	1.0	1.12	1.16	1.07	1.18
350	1.69	1.2	1.13	1.23	1.34	1.11	1.18	1.2	1.13	1.49	1.23	1.0	1.1	1.05	1.19
370	1.68	1.23	1.14	1.24	1.37	1.1	1.19	1.21	1.12	1.49	1.25	1.09	1.0	1.04	1.18
375	1.7	1.25	1.18	1.27	1.37	1.15	1.21	1.23	1.17	1.52	1.27	1.15	1.14	1.0	1.22
380	1.51	1.11	1.08	1.12	1.21	1.04	1.09	1.1	1.05	1.32	1.12	1.03	1.05	0.99	1.0

Table 18: Relative nRMSE RF.

	235	240	260	269	270	275	279	280	290	310	344	350	370	375	380
235	0.47	0.45	0.47	0.45	0.42	0.47	0.45	0.45	0.46	0.45	0.46	0.47	0.47	0.44	0.49
240	0.57	0.38	0.42	0.42	0.44	0.42	0.41	0.42	0.43	0.49	0.42	0.42	0.43	0.4	0.45
260	0.61	0.43	0.38	0.44	0.48	0.41	0.42	0.44	0.42	0.53	0.44	0.4	0.41	0.38	0.44
269	0.56	0.42	0.43	0.38	0.44	0.42	0.41	0.41	0.43	0.49	0.42	0.42	0.43	0.4	0.44
270	0.51	0.44	0.45	0.43	0.37	0.46	0.43	0.42	0.46	0.48	0.44	0.46	0.47	0.43	0.48
275	0.61	0.44	0.42	0.44	0.48	0.37	0.42	0.44	0.41	0.53	0.45	0.4	0.4	0.38	0.43
279	0.57	0.42	0.42	0.42	0.44	0.42	0.37	0.41	0.43	0.5	0.43	0.42	0.43	0.39	0.44
280	0.55	0.42	0.42	0.42	0.42	0.42	0.41	0.38	0.43	0.49	0.43	0.42	0.43	0.4	0.45
290	0.59	0.44	0.41	0.44	0.47	0.4	0.42	0.43	0.37	0.52	0.44	0.4	0.4	0.38	0.43
310	0.52	0.44	0.46	0.45	0.43	0.47	0.45	0.45	0.46	0.38	0.45	0.47	0.47	0.44	0.48
344	0.57	0.41	0.42	0.42	0.44	0.43	0.42	0.42	0.43	0.49	0.38	0.42	0.43	0.4	0.44
350	0.61	0.44	0.41	0.44	0.49	0.4	0.43	0.44	0.41	0.54	0.45	0.36	0.4	0.38	0.43
370	0.62	0.45	0.42	0.46	0.5	0.4	0.44	0.45	0.41	0.55	0.46	0.4	0.37	0.38	0.44
375	0.6	0.44	0.41	0.44	0.48	0.4	0.43	0.43	0.41	0.53	0.45	0.4	0.4	0.35	0.43
380	0.59	0.44	0.42	0.44	0.47	0.41	0.43	0.43	0.41	0.52	0.44	0.41	0.41	0.39	0.39

Table 19: Absolute nRMSE RF.

	235	240	260	269	270	275	279	280	290	310	344	350	370	375	380
235	1.0	0.89	0.89	0.88	0.85	0.9	0.86	0.85	0.89	1.0	0.9	0.92	0.93	0.92	0.97
240	1.43	1.0	1.0	1.01	1.1	1.02	0.99	0.99	1.03	1.27	1.04	1.03	1.05	1.04	1.08
260	1.59	1.09	1.0	1.09	1.23	1.04	1.04	1.06	1.05	1.43	1.12	1.05	1.07	1.06	1.13
269	1.44	1.07	1.04	1.0	1.11	1.05	1.0	1.01	1.07	1.32	1.07	1.08	1.09	1.07	1.11
270	1.32	1.09	1.08	1.04	1.0	1.11	1.02	1.01	1.11	1.28	1.09	1.14	1.17	1.12	1.18
275	1.58	1.12	1.05	1.09	1.24	1.0	1.05	1.07	1.06	1.44	1.15	1.05	1.05	1.06	1.11
279	1.51	1.1	1.07	1.05	1.15	1.05	1.0	1.03	1.08	1.37	1.13	1.09	1.11	1.09	1.14
280	1.48	1.1	1.07	1.06	1.12	1.07	1.01	1.0	1.09	1.37	1.12	1.1	1.13	1.1	1.15
290	1.53	1.1	1.02	1.07	1.2	1.0	1.0	1.02	1.0	1.4	1.12	1.03	1.03	1.03	1.08
310	1.21	0.98	0.99	0.97	0.99	1.0	0.95	0.95	1.0	1.0	0.99	1.04	1.04	1.02	1.03
344	1.43	1.02	1.0	1.0	1.09	1.03	0.99	0.99	1.04	1.29	1.0	1.06	1.08	1.06	1.1
350	1.59	1.11	1.02	1.09	1.25	1.0	1.02	1.05	1.02	1.45	1.14	1.0	1.03	1.05	1.1
370	1.58	1.12	1.03	1.1	1.27	1.0	1.03	1.07	1.02	1.46	1.15	1.05	1.0	1.04	1.09
375	1.53	1.09	1.01	1.06	1.21	1.0	1.0	1.03	1.01	1.41	1.12	1.03	1.03	1.0	1.07
380	1.45	1.05	0.99	1.02	1.15	0.97	0.97	0.99	0.98	1.33	1.07	1.01	1.0	1.0	1.0

Table 20: Relative MAE XGB.

	235	240	260	269	270	275	279	280	290	310	344	350	370	375	380
235	26.64	23.76	23.6	23.4	22.72	23.85	22.8	22.71	23.75	26.55	24.1	24.54	24.86	24.44	25.74
240	29.92	20.86	20.82	21.06	22.99	21.28	20.64	20.71	21.55	26.46	21.6	21.56	21.91	21.74	22.56
260	31.44	21.62	19.82	21.6	24.31	20.63	20.57	20.98	20.9	28.42	22.22	20.72	21.16	21.06	22.31
269	29.61	21.86	21.41	20.49	22.75	21.59	20.58	20.63	21.92	27.11	22.02	22.08	22.39	22.01	22.84
270	28.05	23.21	22.94	22.0	21.24	23.56	21.74	21.41	23.66	27.19	23.12	24.26	24.9	23.89	25.15
275	31.84	22.61	21.05	22.0	24.92	20.12	21.05	21.47	21.27	28.96	23.1	21.06	21.17	21.29	22.32
279	30.37	22.06	21.36	21.13	23.09	21.09	20.05	20.63	21.74	27.54	22.64	21.92	22.27	21.76	22.77
280	29.81	22.22	21.57	21.26	22.53	21.47	20.39	20.12	21.97	27.52	22.57	22.13	22.64	22.13	23.2
290	31.15	22.43	20.74	21.81	24.44	20.37	20.42	20.9	20.4	28.63	22.92	20.95	21.05	20.97	22.07
310	28.65	23.2	23.39	23.0	23.38	23.65	22.54	22.57	23.73	23.73	23.57	24.59	24.75	24.15	24.54
344	29.88	21.37	20.96	20.89	22.78	21.6	20.7	20.7	21.67	26.91	20.91	22.15	22.49	22.08	22.91
350	31.93	22.2	20.48	21.81	25.1	20.11	20.55	21.16	20.57	29.18	22.98	20.08	20.69	21.03	22.05
370	31.91	22.61	20.72	22.19	25.53	20.17	20.78	21.54	20.55	29.5	23.22	21.06	20.14	20.96	21.98
375	31.36	22.38	20.74	21.8	24.71	20.39	20.48	21.16	20.65	28.92	22.89	21.16	21.04	20.49	21.91
380	30.87	22.41	21.13	21.69	24.53	20.6	20.72	21.14	20.92	28.23	22.76	21.53	21.41	21.37	21.31

Table 21: Absolute MAE XGB .

68

	235	240	260	269	270	275	279	280	290	310	344	350	370	375	380
235	1.0	0.9	0.9	0.89	0.86	0.91	0.87	0.87	0.9	0.99	0.9	0.93	0.93	0.92	0.97
240	1.47	1.0	1.0	1.03	1.12	1.03	1.01	1.01	1.04	1.31	1.04	1.03	1.05	1.04	1.1
260	1.64	1.1	1.0	1.11	1.25	1.05	1.06	1.08	1.06	1.48	1.13	1.04	1.06	1.06	1.13
269	1.47	1.06	1.04	1.0	1.12	1.06	1.01	1.02	1.07	1.35	1.07	1.07	1.08	1.07	1.11
270	1.32	1.08	1.08	1.04	1.0	1.12	1.03	1.02	1.12	1.28	1.08	1.14	1.16	1.12	1.18
275	1.63	1.13	1.04	1.12	1.27	1.0	1.06	1.09	1.06	1.49	1.15	1.03	1.04	1.05	1.12
279	1.54	1.08	1.05	1.06	1.15	1.04	1.0	1.03	1.07	1.4	1.11	1.07	1.08	1.06	1.13
280	1.49	1.08	1.05	1.05	1.12	1.06	1.01	1.0	1.08	1.38	1.1	1.08	1.09	1.07	1.13
290	1.57	1.1	1.0	1.08	1.22	1.0	1.02	1.04	1.0	1.44	1.12	1.01	1.01	1.01	1.08
310	1.22	0.99	0.99	0.99	0.99	1.01	0.96	0.97	1.01	1.0	1.0	1.04	1.05	1.02	1.05
344	1.47	1.02	1.01	1.01	1.11	1.05	1.01	1.01	1.04	1.31	1.0	1.06	1.07	1.05	1.1
350	1.65	1.12	1.03	1.12	1.28	1.01	1.05	1.08	1.04	1.51	1.16	1.0	1.03	1.05	1.12
370	1.65	1.15	1.04	1.14	1.31	1.02	1.07	1.1	1.04	1.52	1.18	1.05	1.0	1.04	1.12
375	1.6	1.11	1.01	1.09	1.24	1.0	1.03	1.06	1.02	1.47	1.13	1.03	1.02	1.0	1.09
380	1.47	1.04	0.97	1.02	1.16	0.96	0.98	0.99	0.97	1.34	1.06	0.99	0.98	0.98	1.0

Table 22: Relative RMSE XGB.

	235	240	260	269	270	275	279	280	290	310	344	350	370	375	380
235	37.3	33.39	33.41	33.05	32.17	33.92	32.51	32.48	33.69	36.84	33.76	34.52	34.81	34.29	36.15
240	44.02	29.95	29.98	30.77	33.52	30.95	30.25	30.39	31.24	39.15	31.02	30.95	31.41	31.19	32.8
260	47.4	31.6	28.85	31.99	36.07	30.2	30.54	31.25	30.63	42.84	32.49	30.05	30.59	30.44	32.66
269	43.28	31.09	30.57	29.38	32.8	31.01	29.81	29.92	31.36	39.77	31.31	31.3	31.72	31.29	32.66
270	39.93	32.5	32.53	31.48	30.14	33.68	31.18	30.72	33.67	38.45	32.55	34.24	35.07	33.74	35.58
275	47.27	32.68	30.12	32.32	36.61	28.92	30.72	31.56	30.61	43.23	33.34	29.92	29.94	30.32	32.27
279	44.46	31.39	30.31	30.6	33.28	30.24	28.96	29.94	31.05	40.49	32.21	31.02	31.36	30.71	32.64
280	43.47	31.3	30.53	30.55	32.47	30.78	29.4	29.1	31.3	40.23	31.89	31.3	31.83	31.21	32.94
290	46.29	32.33	29.64	31.92	35.87	29.52	29.99	30.69	29.52	42.54	33.04	29.92	29.96	29.96	32.0
310	40.52	32.87	33.11	32.9	32.93	33.67	32.17	32.33	33.56	33.34	33.32	34.72	34.84	33.87	35.17
344	43.84	30.51	30.13	30.37	33.18	31.3	30.26	30.3	31.13	39.31	29.93	31.62	32.0	31.5	32.97
350	47.91	32.52	29.77	32.4	37.23	29.37	30.58	31.37	30.04	43.8	33.77	29.02	29.77	30.38	32.41
370	47.88	33.17	30.05	33.03	37.96	29.5	30.96	31.95	30.09	44.11	34.17	30.48	28.97	30.26	32.35
375	46.83	32.54	29.77	32.11	36.38	29.47	30.09	31.05	29.84	43.08	33.27	30.36	29.97	29.34	31.87
380	45.6	32.15	30.14	31.65	35.73	29.7	30.17	30.77	30.03	41.56	32.69	30.69	30.45	30.3	30.93

Table 23: Absolute RMSE XGB.

	235	240	260	269	270	275	279	280	290	310	344	350	370	375	380
235	1.0	0.94	0.98	0.96	0.9	0.99	0.95	0.96	0.97	0.98	0.96	0.98	1.0	0.92	1.04
240	1.41	1.0	1.04	1.05	1.11	1.06	1.04	1.06	1.06	1.23	1.04	1.04	1.06	0.99	1.11
260	1.51	1.06	1.0	1.09	1.19	1.04	1.05	1.08	1.04	1.34	1.09	1.01	1.03	0.97	1.1
269	1.38	1.04	1.06	1.0	1.08	1.06	1.02	1.04	1.06	1.24	1.04	1.05	1.07	0.99	1.1
270	1.28	1.1	1.14	1.08	1.0	1.16	1.08	1.07	1.15	1.21	1.1	1.16	1.19	1.08	1.21
275	1.52	1.11	1.06	1.11	1.21	1.0	1.06	1.1	1.05	1.36	1.12	1.01	1.02	0.97	1.1
279	1.43	1.06	1.06	1.05	1.1	1.05	1.0	1.04	1.06	1.27	1.08	1.04	1.06	0.98	1.11
280	1.37	1.04	1.05	1.03	1.06	1.05	1.02	1.0	1.05	1.25	1.06	1.04	1.06	0.98	1.1
290	1.47	1.08	1.03	1.09	1.17	1.01	1.05	1.06	1.0	1.33	1.1	1.0	1.01	0.95	1.08
310	1.24	1.06	1.11	1.08	1.04	1.11	1.09	1.08	1.11	1.0	1.07	1.12	1.13	1.03	1.14
344	1.4	1.02	1.05	1.04	1.09	1.08	1.06	1.05	1.07	1.23	1.0	1.06	1.08	1.0	1.11
350	1.57	1.12	1.07	1.14	1.26	1.04	1.11	1.12	1.06	1.41	1.16	1.0	1.03	0.99	1.13
370	1.56	1.14	1.07	1.15	1.27	1.04	1.11	1.13	1.06	1.41	1.17	1.03	1.0	0.98	1.12
375	1.61	1.17	1.11	1.18	1.28	1.09	1.14	1.16	1.1	1.45	1.19	1.08	1.08	1.0	1.16
380	1.39	1.03	1.0	1.03	1.12	0.98	1.02	1.02	0.99	1.24	1.04	0.97	0.98	0.93	1.0

Table 24: Relative nRMSE XGB.

	235	240	260	269	270	275	279	280	290	310	344	350	370	375	380
235	0.46	0.44	0.46	0.44	0.42	0.46	0.44	0.44	0.45	0.45	0.45	0.46	0.46	0.43	0.48
240	0.55	0.39	0.41	0.41	0.44	0.42	0.41	0.42	0.42	0.48	0.41	0.41	0.42	0.39	0.44
260	0.6	0.42	0.39	0.43	0.47	0.41	0.41	0.43	0.41	0.53	0.43	0.4	0.41	0.38	0.44
269	0.55	0.41	0.42	0.4	0.43	0.42	0.4	0.41	0.42	0.49	0.41	0.41	0.42	0.39	0.44
270	0.5	0.43	0.45	0.42	0.39	0.46	0.42	0.42	0.45	0.47	0.43	0.45	0.47	0.42	0.47
275	0.6	0.43	0.41	0.44	0.47	0.39	0.42	0.43	0.41	0.53	0.44	0.4	0.4	0.38	0.43
279	0.56	0.42	0.42	0.41	0.43	0.41	0.39	0.41	0.42	0.5	0.42	0.41	0.42	0.38	0.43
280	0.55	0.41	0.42	0.41	0.42	0.42	0.41	0.4	0.42	0.5	0.42	0.41	0.42	0.39	0.44
290	0.58	0.43	0.41	0.43	0.46	0.4	0.42	0.42	0.4	0.52	0.44	0.4	0.4	0.37	0.43
310	0.51	0.44	0.45	0.44	0.43	0.46	0.45	0.44	0.45	0.41	0.44	0.46	0.46	0.42	0.47
344	0.55	0.4	0.41	0.41	0.43	0.43	0.42	0.41	0.42	0.48	0.39	0.42	0.43	0.39	0.44
350	0.6	0.43	0.41	0.44	0.48	0.4	0.42	0.43	0.41	0.54	0.44	0.38	0.4	0.38	0.43
370	0.6	0.44	0.41	0.44	0.49	0.4	0.43	0.44	0.41	0.54	0.45	0.4	0.39	0.38	0.43
375	0.59	0.43	0.41	0.43	0.47	0.4	0.42	0.42	0.4	0.53	0.44	0.4	0.4	0.37	0.42
380	0.57	0.43	0.41	0.43	0.46	0.4	0.42	0.42	0.41	0.51	0.43	0.4	0.4	0.38	0.41

Table 25: Absolute nRMSE XGB.

	235	240	260	269	270	275	279	280	290	310	344	350	370	375	380
235	1.0	0.91	0.89	0.92	0.9	0.93	0.93	0.91	0.92	1.0	0.91	0.92	0.92	0.92	0.95
240	1.34	1.0	0.99	1.01	1.05	1.03	1.02	1.02	1.05	1.25	1.03	1.03	1.03	1.04	1.08
260	1.44	1.08	1.0	1.07	1.12	1.07	1.05	1.06	1.07	1.33	1.1	1.05	1.07	1.06	1.12
269	1.33	1.03	0.99	1.0	1.06	1.04	1.02	1.03	1.03	1.23	1.04	1.02	1.01	1.01	1.05
270	1.33	1.03	1.0	1.03	1.0	1.05	1.04	1.02	1.06	1.3	1.04	1.06	1.05	1.08	1.13
275	1.43	1.08	1.01	1.06	1.12	1.0	1.03	1.06	1.03	1.31	1.1	1.02	1.01	1.03	1.09
279	1.44	1.07	1.01	1.05	1.1	1.0	1.0	1.02	1.04	1.35	1.1	1.03	1.04	1.05	1.12
280	1.43	1.06	1.01	1.02	1.07	1.02	1.0	1.0	1.05	1.35	1.08	1.04	1.04	1.08	1.12
290	1.46	1.1	1.02	1.07	1.13	1.01	1.01	1.03	1.0	1.36	1.12	1.02	1.01	1.04	1.09
310	1.19	0.99	0.96	1.0	1.02	0.99	0.99	0.99	0.99	1.0	0.98	0.99	0.97	0.98	1.0
344	1.36	1.03	1.0	1.03	1.04	1.05	1.03	1.03	1.05	1.27	1.0	1.04	1.05	1.05	1.09
350	1.42	1.09	1.02	1.06	1.11	1.02	1.03	1.03	1.03	1.33	1.12	1.0	1.02	1.04	1.09
370	1.48	1.13	1.04	1.09	1.17	1.0	1.03	1.05	1.02	1.43	1.16	1.04	1.0	1.07	1.11
375	1.44	1.09	1.01	1.08	1.14	1.01	1.03	1.06	1.01	1.34	1.12	1.01	1.0	1.0	1.06
380	1.34	1.05	1.0	1.03	1.06	1.02	1.01	1.03	1.0	1.25	1.05	1.0	1.0	0.99	1.0

Table 26: Relative MAE ANN.

73

	235	240	260	269	270	275	279	280	290	310	344	350	370	375	380
235	25.61	23.23	22.8	23.5	22.99	23.83	23.71	23.43	23.48	25.5	23.35	23.64	23.44	23.63	24.28
240	27.45	20.42	20.16	20.69	21.43	21.1	20.89	20.83	21.34	25.44	20.94	21.04	20.99	21.16	22.05
260	28.08	21.15	19.54	21.0	21.87	20.83	20.5	20.73	21.0	25.9	21.41	20.59	20.91	20.79	21.91
269	28.0	21.62	20.91	21.03	22.26	21.85	21.54	21.75	21.7	25.81	21.91	21.44	21.25	21.3	22.05
270	26.86	20.83	20.26	20.74	20.21	21.25	21.02	20.59	21.48	26.19	20.96	21.46	21.24	21.73	22.8
275	28.37	21.43	20.06	21.05	22.13	19.83	20.52	20.99	20.52	26.02	21.89	20.3	20.07	20.42	21.53
279	28.49	21.24	20.04	20.82	21.87	19.91	19.85	20.32	20.69	26.72	21.88	20.38	20.58	20.92	22.18
280	28.15	20.87	19.95	20.19	21.06	20.16	19.72	19.75	20.76	26.59	21.38	20.59	20.56	21.25	22.07
290	28.92	21.78	20.13	21.13	22.29	19.94	19.96	20.41	19.74	26.8	22.17	20.19	19.96	20.47	21.46
310	27.65	22.87	22.25	23.11	23.56	23.06	22.9	22.97	22.91	23.2	22.69	22.92	22.56	22.68	23.16
344	28.07	21.14	20.64	21.29	21.41	21.71	21.24	21.18	21.61	26.18	20.59	21.49	21.68	21.6	22.47
350	27.66	21.13	19.78	20.7	21.53	19.95	19.95	20.09	20.03	25.9	21.77	19.46	19.85	20.22	21.15
370	29.27	22.38	20.55	21.6	23.24	19.71	20.38	20.81	20.25	28.25	23.06	20.57	19.81	21.17	21.93
375	28.83	21.95	20.33	21.59	22.87	20.22	20.62	21.15	20.33	26.8	22.5	20.25	20.11	20.05	21.32
380	28.43	22.16	21.11	21.84	22.41	21.6	21.47	21.75	21.24	26.4	22.22	21.22	21.23	21.05	21.16

Table 27: Absolute MAE ANN.

	235	240	260	269	270	275	279	280	290	310	344	350	370	375	380
235	1.0	0.91	0.9	0.92	0.9	0.93	0.92	0.92	0.92	0.99	0.91	0.92	0.92	0.92	0.96
240	1.33	1.0	1.0	1.01	1.04	1.04	1.02	1.02	1.05	1.26	1.02	1.03	1.03	1.04	1.1
260	1.4	1.07	1.0	1.07	1.09	1.06	1.04	1.05	1.07	1.32	1.08	1.05	1.07	1.06	1.14
269	1.31	1.03	1.0	1.0	1.05	1.04	1.02	1.03	1.03	1.23	1.04	1.02	1.01	1.01	1.07
270	1.32	1.04	1.02	1.04	1.0	1.06	1.05	1.02	1.08	1.31	1.04	1.07	1.06	1.08	1.15
275	1.38	1.07	1.01	1.05	1.09	1.0	1.03	1.05	1.03	1.3	1.08	1.02	1.01	1.02	1.1
279	1.42	1.08	1.02	1.05	1.09	1.0	1.0	1.02	1.06	1.37	1.11	1.03	1.04	1.06	1.14
280	1.39	1.06	1.02	1.03	1.05	1.03	1.01	1.0	1.06	1.36	1.08	1.04	1.05	1.07	1.14
290	1.42	1.09	1.02	1.06	1.1	1.0	1.0	1.02	1.0	1.35	1.1	1.01	1.01	1.03	1.1
310	1.19	0.99	0.96	1.01	1.01	0.99	0.99	0.99	0.99	1.0	0.98	0.99	0.98	0.97	1.02
344	1.35	1.03	1.01	1.04	1.04	1.06	1.04	1.03	1.05	1.29	1.0	1.04	1.05	1.05	1.11
350	1.38	1.07	1.02	1.06	1.08	1.02	1.02	1.03	1.03	1.32	1.1	1.0	1.02	1.03	1.1
370	1.43	1.12	1.03	1.08	1.14	0.99	1.02	1.03	1.03	1.42	1.15	1.04	1.0	1.06	1.12
375	1.39	1.09	1.02	1.07	1.11	1.01	1.02	1.04	1.02	1.32	1.11	1.02	1.01	1.0	1.09
380	1.3	1.03	0.98	1.01	1.03	1.0	1.0	1.01	0.99	1.23	1.03	0.99	0.99	0.98	1.0

Table 28: Relative RMSE ANN.

	235	240	260	269	270	275	279	280	290	310	344	350	370	375	380
235	37.29	33.95	33.58	34.19	33.69	34.72	34.42	34.25	34.31	36.8	34.01	34.46	34.15	34.24	35.71
240	39.57	29.8	29.72	30.15	30.98	30.97	30.47	30.24	31.33	37.48	30.31	30.69	30.81	30.92	32.79
260	40.18	30.72	28.76	30.65	31.33	30.54	29.92	30.23	30.82	38.07	31.19	30.24	30.79	30.35	32.66
269	39.71	31.19	30.25	30.23	31.84	31.47	30.92	31.21	31.26	37.2	31.32	30.77	30.61	30.61	32.2
270	39.6	31.14	30.46	31.09	30.0	31.77	31.47	30.75	32.26	39.44	31.08	31.99	31.79	32.42	34.51
275	40.59	31.38	29.75	31.01	32.06	29.4	30.23	30.9	30.42	38.13	31.88	29.86	29.75	30.01	32.35
279	41.19	31.17	29.51	30.56	31.59	29.02	28.96	29.59	30.56	39.75	32.03	29.86	30.23	30.63	33.12
280	40.98	31.09	29.99	30.21	30.96	30.26	29.56	29.4	31.26	39.98	31.74	30.67	30.87	31.53	33.42
290	41.43	31.82	29.76	31.02	32.19	29.33	29.37	29.88	29.26	39.46	32.26	29.69	29.6	30.09	32.08
310	39.59	33.03	32.11	33.5	33.63	33.04	33.02	33.06	33.0	33.31	32.62	33.06	32.53	32.41	34.1
344	40.41	30.77	30.19	30.93	30.98	31.54	30.9	30.73	31.4	38.51	29.83	31.17	31.46	31.27	33.09
350	39.81	30.92	29.33	30.5	31.18	29.49	29.44	29.57	29.68	38.15	31.81	28.81	29.47	29.78	31.78
370	42.87	33.35	30.89	32.36	34.18	29.54	30.55	30.92	30.72	42.47	34.37	30.95	29.89	31.64	33.62
375	40.77	31.83	29.86	31.3	32.64	29.61	30.05	30.58	29.85	38.8	32.63	29.85	29.72	29.32	31.84
380	40.51	31.97	30.66	31.6	32.22	31.31	31.12	31.41	30.77	38.43	32.05	30.77	30.96	30.62	31.15

Table 29: Absolute RMSE ANN.

	235	240	260	269	270	275	279	280	290	310	344	350	370	375	380
235	1.0	0.96	0.99	0.99	0.94	1.01	1.0	1.01	0.99	0.98	0.97	0.98	0.98	0.92	1.02
240	1.27	1.0	1.04	1.04	1.03	1.07	1.06	1.06	1.07	1.18	1.02	1.04	1.05	0.99	1.12
260	1.29	1.03	1.0	1.05	1.03	1.05	1.03	1.05	1.05	1.19	1.05	1.02	1.04	0.97	1.11
269	1.23	1.02	1.02	1.0	1.02	1.05	1.03	1.05	1.03	1.13	1.02	1.0	1.0	0.94	1.06
270	1.28	1.06	1.07	1.07	1.0	1.1	1.1	1.08	1.11	1.25	1.05	1.09	1.09	1.04	1.18
275	1.28	1.04	1.03	1.05	1.04	1.0	1.03	1.06	1.02	1.18	1.06	0.99	1.0	0.94	1.08
279	1.32	1.05	1.03	1.05	1.04	1.0	1.0	1.03	1.04	1.25	1.07	1.0	1.03	0.98	1.12
280	1.28	1.02	1.02	1.01	1.0	1.02	1.02	1.0	1.04	1.23	1.04	1.01	1.02	0.98	1.11
290	1.33	1.08	1.04	1.07	1.06	1.02	1.04	1.04	1.0	1.24	1.08	1.0	1.01	0.96	1.09
310	1.21	1.07	1.07	1.1	1.06	1.09	1.12	1.1	1.09	1.0	1.05	1.06	1.06	0.99	1.11
344	1.29	1.04	1.05	1.06	1.02	1.09	1.09	1.07	1.08	1.21	1.0	1.05	1.07	1.0	1.12
350	1.32	1.08	1.06	1.08	1.06	1.05	1.07	1.06	1.05	1.23	1.1	1.0	1.03	0.98	1.11
370	1.36	1.11	1.07	1.09	1.11	1.01	1.07	1.06	1.04	1.31	1.14	1.02	1.0	0.99	1.12
375	1.4	1.15	1.12	1.15	1.15	1.1	1.14	1.14	1.1	1.3	1.17	1.06	1.08	1.0	1.16
380	1.23	1.02	1.01	1.03	1.0	1.03	1.04	1.04	1.0	1.14	1.02	0.97	0.99	0.93	1.0

Table 30: Relative nRMSE ANN.

	235	240	260	269	270	275	279	280	290	310	344	350	370	375	380
235	0.46	0.45	0.46	0.46	0.44	0.47	0.47	0.47	0.46	0.45	0.45	0.46	0.45	0.43	0.48
240	0.5	0.39	0.41	0.41	0.4	0.42	0.41	0.41	0.42	0.46	0.4	0.41	0.41	0.39	0.44
260	0.51	0.41	0.39	0.41	0.41	0.41	0.41	0.41	0.41	0.47	0.41	0.4	0.41	0.38	0.44
269	0.5	0.41	0.42	0.41	0.41	0.43	0.42	0.43	0.42	0.46	0.41	0.41	0.41	0.38	0.43
270	0.5	0.41	0.42	0.42	0.39	0.43	0.43	0.42	0.43	0.49	0.41	0.42	0.42	0.41	0.46
275	0.51	0.42	0.41	0.42	0.42	0.4	0.41	0.42	0.41	0.47	0.42	0.39	0.4	0.38	0.43
279	0.52	0.41	0.41	0.41	0.41	0.39	0.39	0.4	0.41	0.49	0.42	0.39	0.4	0.38	0.44
280	0.52	0.41	0.41	0.41	0.4	0.41	0.41	0.4	0.42	0.49	0.42	0.41	0.41	0.39	0.45
290	0.52	0.42	0.41	0.42	0.42	0.4	0.41	0.41	0.39	0.49	0.43	0.39	0.39	0.38	0.43
310	0.5	0.44	0.44	0.45	0.44	0.45	0.46	0.45	0.45	0.41	0.43	0.44	0.43	0.41	0.45
344	0.51	0.41	0.41	0.42	0.4	0.43	0.43	0.42	0.43	0.47	0.39	0.41	0.42	0.39	0.44
350	0.5	0.41	0.4	0.41	0.4	0.4	0.41	0.4	0.4	0.47	0.42	0.38	0.39	0.37	0.42
370	0.54	0.44	0.42	0.44	0.44	0.4	0.42	0.42	0.42	0.52	0.45	0.41	0.4	0.4	0.45
375	0.51	0.42	0.41	0.42	0.42	0.4	0.42	0.42	0.4	0.48	0.43	0.39	0.39	0.37	0.42
380	0.51	0.42	0.42	0.43	0.42	0.43	0.43	0.43	0.42	0.47	0.42	0.4	0.41	0.39	0.42

Table 31: Absolute nRMSE ANN.

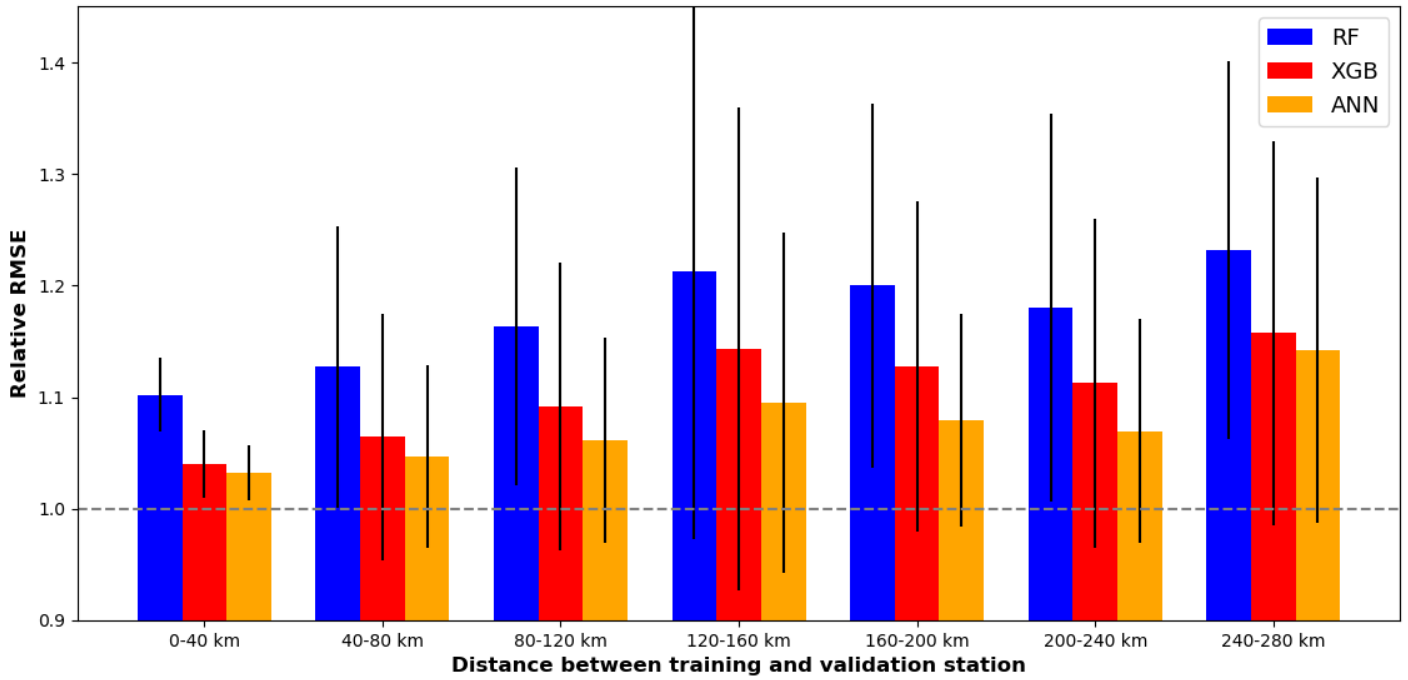# A.4 Distance, cardinal and temporal performance figures

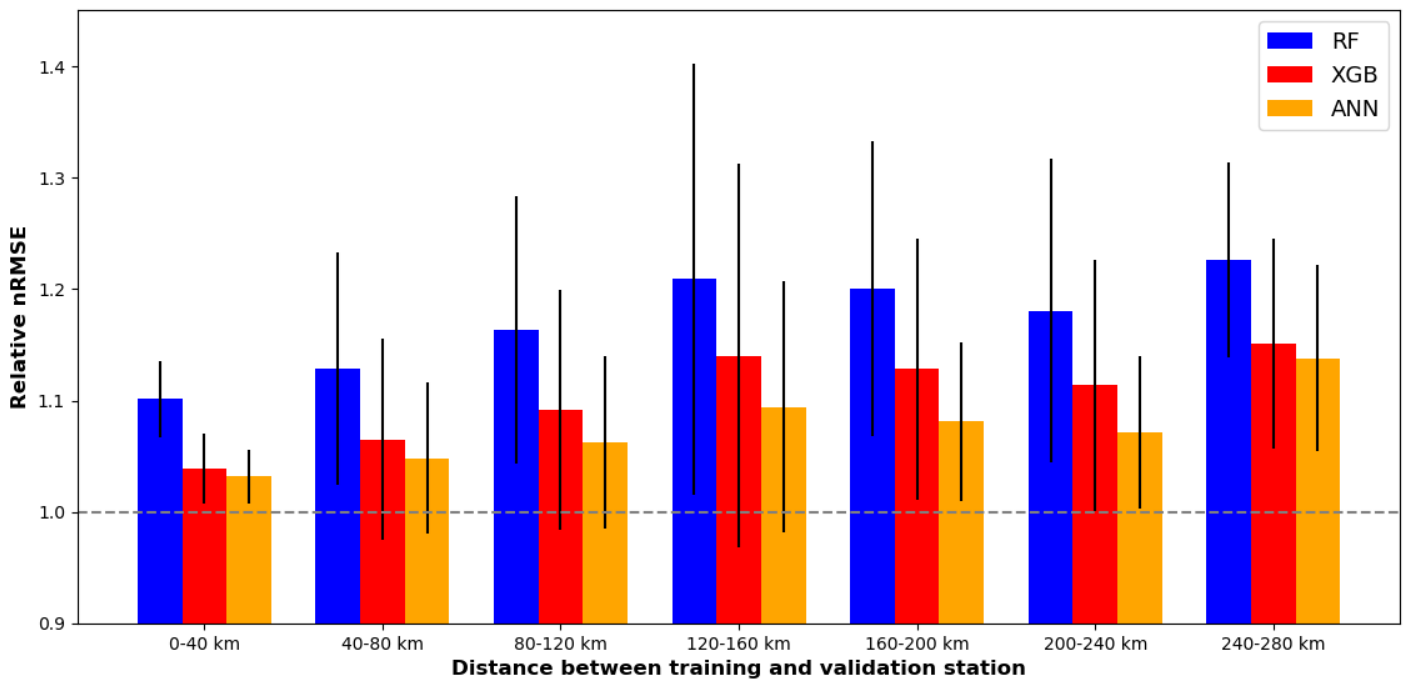Figure 27: Relative RMSE for different distance intervals.

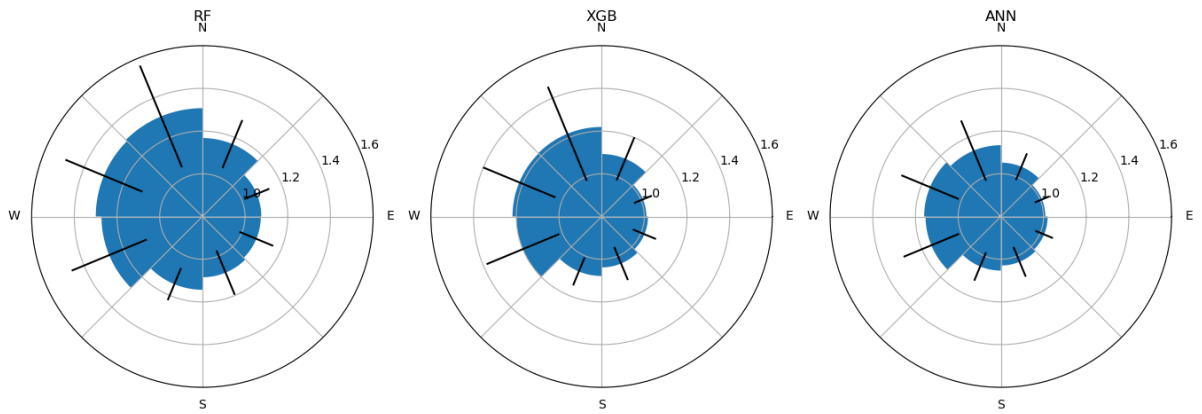Figure 28: Relative nRMSE for different distance intervals.

Figure 29: Cardinal performance of different MLMs based on relative RMSE.
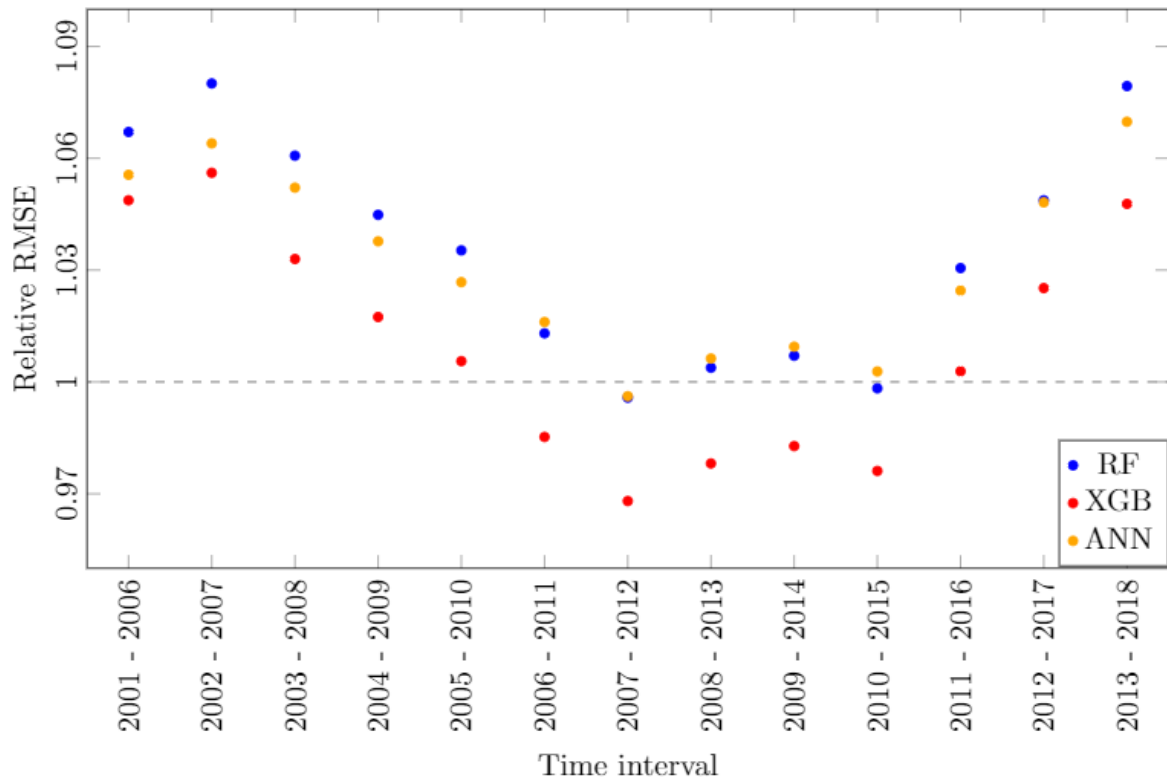

Figure 30: Relative RMSE compared to a reference training interval in the period (2000-2005).
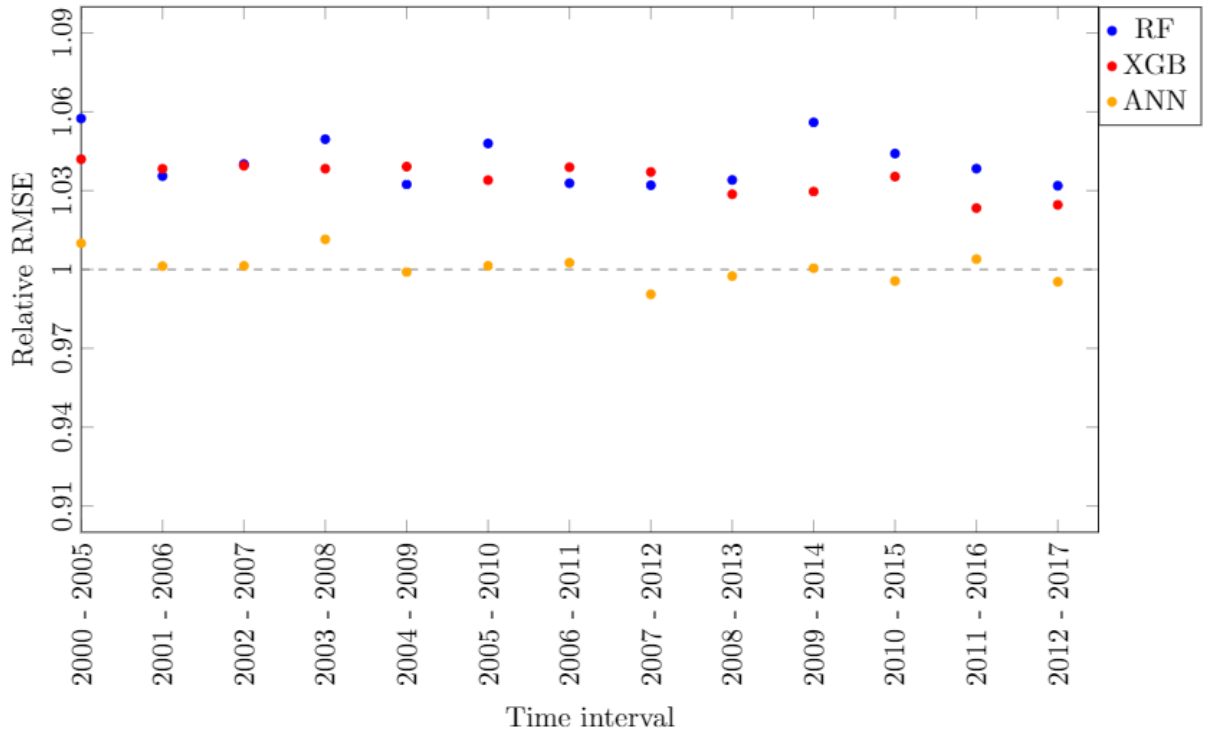
Figure 31: Relative RMSE compared to a reference validation interval in the period (2013-2018).
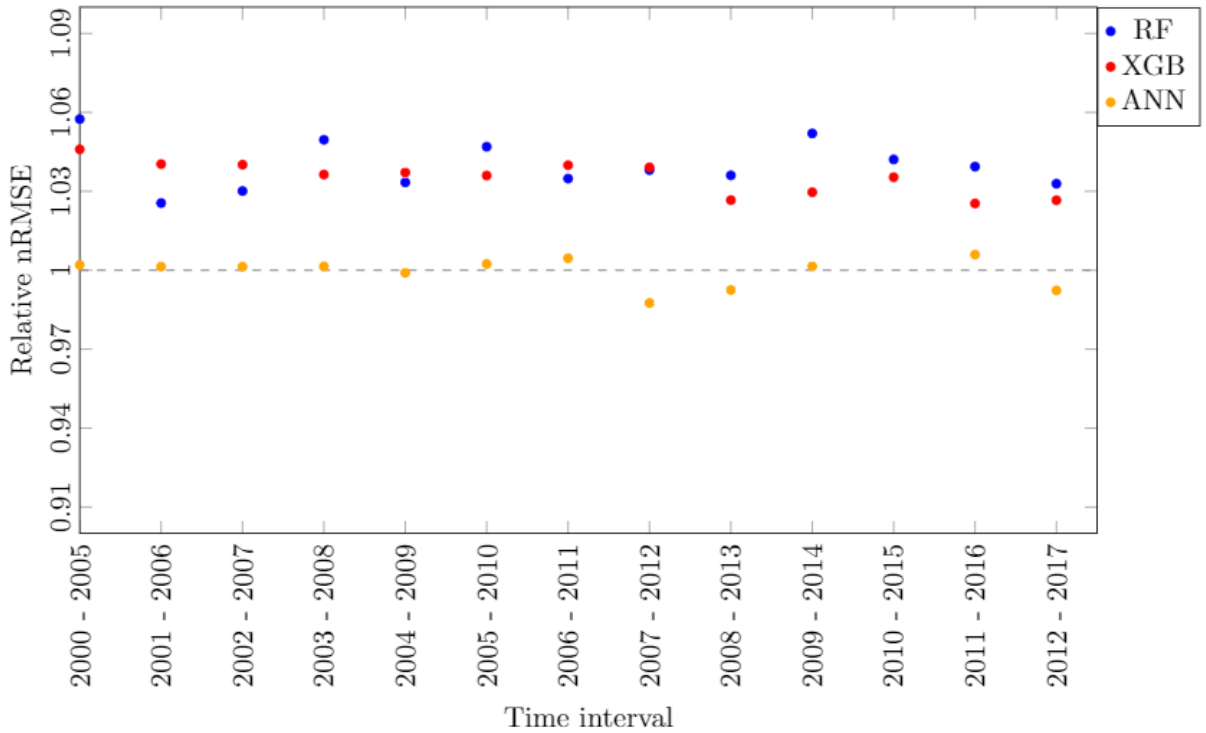

Figure 32: Relative nRMSE compared to a reference validation interval in the period (2013-2018).

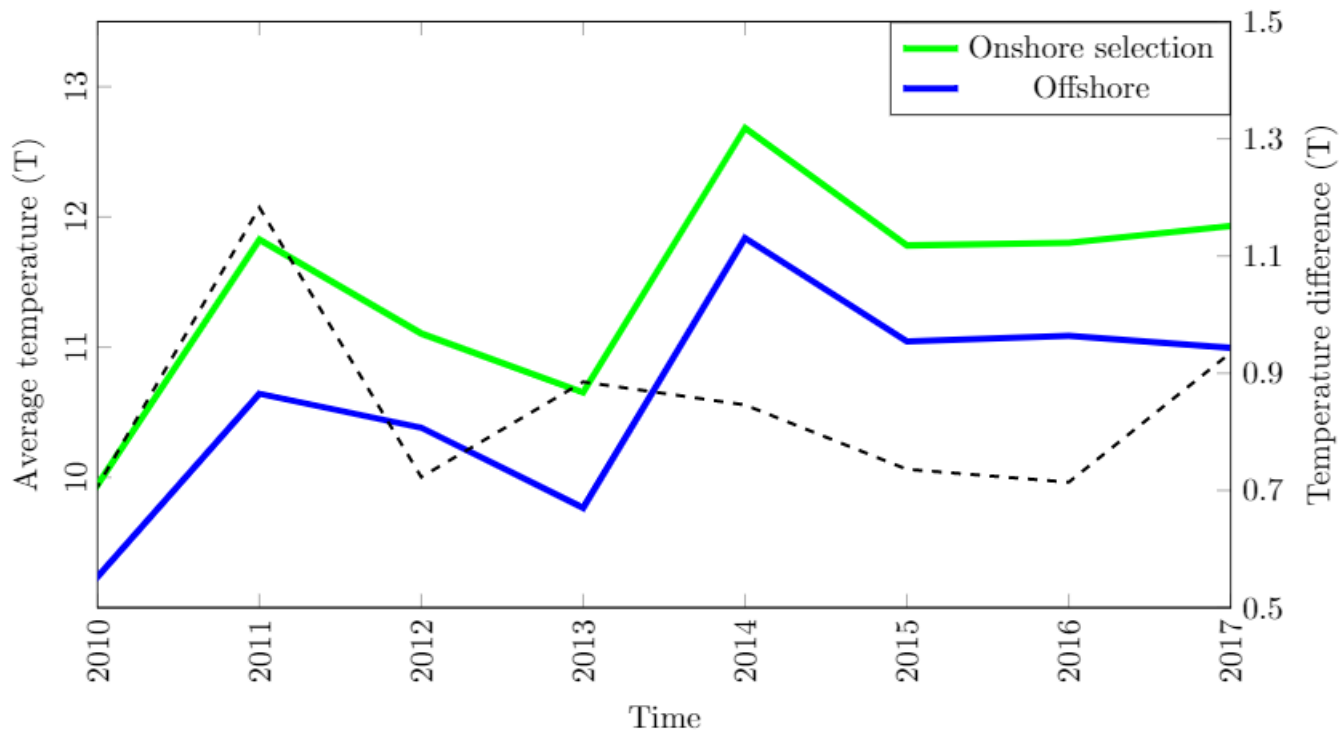## A.5   Onshore and offshore temperatures

Figure 33: Onshore and offshore average temperatures. Black dotted line represents the difference in temperature.